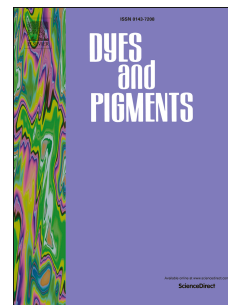


Accepted Manuscript

New conjugated organic dyes with various electron donors: one- and two-photon excited fluorescence, and bioimaging

Feng Jin , Dong-Ling Xu , Hui-Zhi Zhu , Yan Yan , Jun Zheng , Jun Zhang , Hong-Ping Zhou , Jie-Ying Wu , Yu-Peng Tian



PII: S0143-7208(14)00160-0

DOI: [10.1016/j.dyepig.2014.04.032](https://doi.org/10.1016/j.dyepig.2014.04.032)

Reference: DYPI 4360

To appear in: *Dyes and Pigments*

Received Date: 16 October 2013

Revised Date: 23 February 2014

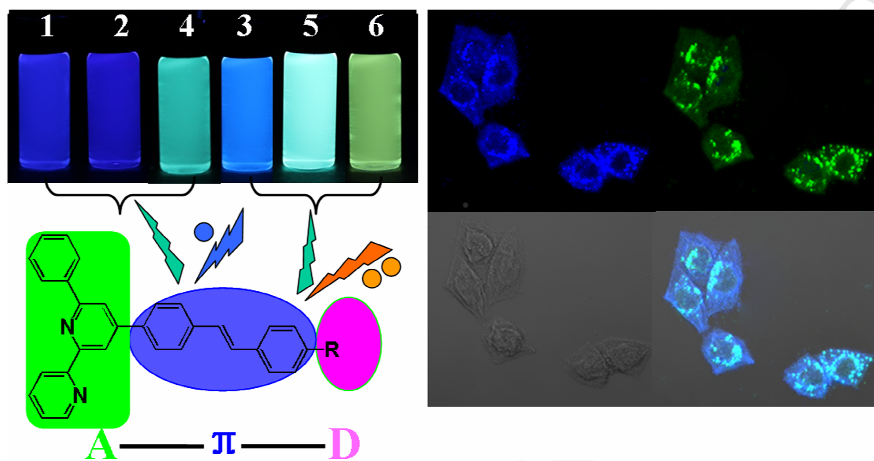
Accepted Date: 22 April 2014

Please cite this article as: Jin F, Xu D-L, Zhu H-Z, Yan Y, Zheng J, Zhang J, Zhou H-P, Wu J-Y, Tian Y-P, New conjugated organic dyes with various electron donors: one- and two-photon excited fluorescence, and bioimaging, *Dyes and Pigments* (2014), doi: 10.1016/j.dyepig.2014.04.032.

This is a PDF file of an unedited manuscript that has been accepted for publication. As a service to our customers we are providing this early version of the manuscript. The manuscript will undergo copyediting, typesetting, and review of the resulting proof before it is published in its final form. Please note that during the production process errors may be discovered which could affect the content, and all legal disclaimers that apply to the journal pertain.

Graphical abstract

One- and two-photon fluorescence of six dyes, being promising in bioimaging applications, were successfully tuned through varying electron donors.



New conjugated organic dyes with various electron donors: one- and two-photon excited fluorescence, and bioimaging

Feng Jin^{a, b}, Dong-Ling Xu^a, Hui-Zhi Zhu^a, Yan Yan^a, Jun Zheng^c, Jun Zhang^a,
Hong-Ping Zhou,^a * Jie-Ying Wu^a, Yu-Peng Tian^a

^aCollege of Chemistry and Chemical Engineering, Anhui University, Hefei 230039, P.

R. China

^bDepartment of Chemistry, Fuyang Normal College, Fuyang 236041, P. R. China

^cCenter of Modern Experimental Technology, Anhui University, Hefei 230039, P. R.

China

*Corresponding author. Fax: +86-551-5107342; Tel: +86-551-5108151

E-mail address: zhpzhp@263.net

ABSTRACT

Six new fluorescent donor- π bridge-acceptor (D- π -A) structural molecules with various electron donors were synthesized and fully characterized. Influence of electron-donating strength on optical properties was investigated by the systematic alteration of the electron donors. The optical properties of the dyes were successfully tuned by choosing different electron donors. All the dyes in solution show strong one-photon excited fluorescence (OPEF) and high quantum yield. With increasing electron-donating strength of donors, dye **5** with diphenylamine and dye **6** with (4,4'-diethoxyphenyl)amino substituents, exhibit strong two-photon excited fluorescence (TPEF), and the large two-photon absorption (TPA) cross-section values

are 1378 GM for **5** and 1654 GM for **6**. The structure-property relationships were detailed through quantum chemical calculations and X-ray crystallography. The results of living cell imaging experiments show the values of them in one- or two-photon fluorescence microscopy bioimaging applications.

Keywords: electron donor, one-photon excited fluorescence, two-photon excited fluorescence, two-photon absorption, structure-property relationship, bioimaging

1. Introduction

Conjugated organic molecules with large delocalized π -electron systems continue to be the subject of very active research due to their potential applications as one- or two- photon optical materials in several areas such as fluorescence imaging, photodynamic therapy, photoswitching devices and 3-D data storage [1-14]. Organic molecules that can be used for such applications are expected to have high fluorescence quantum yield and large two-photon absorption cross-section values. However, the relatively low quantum yield and small two-photon absorption cross-section values of the materials often limit their widespread utility [15-18]. Therefore, extensive efforts have been concentrated on the synthesis of dyes with high fluorescence quantum yield and large two-photon cross-sections. The two-photon absorbing organic materials with large two-photon absorption are particularly attractive due to the advantages of two-photon absorption processes [19]. It is well known that TPA cross-section can be increased either by an enhancement of the conjugation length as well as the coplanarity of the π -center, or by an appropriate combination of electron donors

and acceptors. The molecules with D- π -A structure often have two-photon fluorescence property. It has been well-established that increasing the electron-donating strength of terminal groups and extending conjugation, can exert significant influence on enhancement of TPA cross-section due to the highly extended π -conjugation [20]. Recently, remarkable progress in the design and synthesis of organic dyes with very high TPA cross sections (>1000 GM) has been reported [21].

Dipyridyl has been widely used as electron acceptor group to design optical materials, due to its electron-deficient nature of the heterocycle, excellent optical property, good thermal and chemical stabilities, as well as excellent metal cation coordinationability [22]. Our group has reported a series of TPA pyridine or bipyridine derivatives and the corresponding complexes [23]. As continuous efforts to explore new molecules with high fluorescence quantum yield and large TPA cross section values, 2,2-bipyridyl group as electron acceptor moiety is incorporated into various electron donors through a π -conjugating spacer, we obtained six dyes with excellent optical properties. The adopted electron donors are imidazole (**D1**), triazole (**D2**), carbazole (**D3**), anthracene (**D4**), diphenylamine (**D5**), and (4,4'-diethoxyphenyl)amino (**D6**), whose electron-donating strength increases in the order of **D6** > **D5** > **D3** > **D4** > **D1** > **D2**. By using the different electron donors, the one- and two-photon fluorescence properties of the dyes have been successfully tuned. All the compounds have high fluorescence quantum yield. With increasing electron-donating strength of donors, **5** and **6** exhibit excellent

two-photon excited fluorescence with the maximum TPA cross-section values of 1378 GM for **5** and 1654 GM for **6**, which are relatively large compared to those reported and the commercial fluorophores, such as rhodamine B [24].

The molecular structures for the dyes (**1-6**) are shown in Scheme 1. All the compounds can be obtained in high yield and exhibit a simple preparation and purification at lower cost. In addition, the simple modification of molecular structure by introducing a benzene ring into the six position of pyridyl may produce a steric hindrance, which is expected to suppress molecular internal rotation to some extent and prevent the intermolecular $\pi\cdots\pi$ interactions between the coplanar conjugated backbones. Finally, dyes 1-6 are N^NC-cyclometalated ligands, which are suitable for preparing cyclometalated platinum(II) and ruthenium(II) complexes for use in dye-sensitized solar cells or luminophores [25], and the related studies are currently underway in our group.

Here, we report synthesis and optical properties (linear and nonlinear) of the six organic compounds, together with quantum-chemical calculation and X-ray crystallography for discussion on the correlation between molecular structures and spectral properties. One- and two-photon fluorescence cell imaging experiment indicated the suitability of them for this potential application.

2. Experimental section

2.1. General procedures

All commercially available chemicals are of analytical grade. Every solvent was purified as conventional methods beforehand. Elemental analyses were carried out on Perkin-Elmer 240 analyzer. IR spectra were recorded with a Nicolet FT-IR NEXUS 870 spectrometer (KBr discs) in the 4000-400 cm^{-1} region. ^1H and ^{13}C NMR spectra were recorded on a Bruker AV 400 spectrometer using CDCl_3 or $(\text{CD}_3)_2\text{SO}$ as solvent. Chemical shifts were reported in parts per million (ppm) relative to internal TMS (0 ppm) and coupling constants in Hz. Splitting patterns were described as singlet (s), doublet (d), triplet (t), quartet (q), or multiplet (m). The mass spectra were obtained on a Bruker Autoflex III smartbeam mass spectrometer and a LTQ-Orbitrap XL mass spectrometer. The X-ray diffraction measurements were performed on a CCD area detector using graphite monochromated $\text{MoK}\alpha$ radiation ($\lambda = 0.71069 \text{ \AA}$) at 298 (2) K. Intensity data were collected in the variable ω -scan mode. The structures were solved by direct methods and difference Fourier syntheses. The non-hydrogen atoms were refined anisotropically and hydrogen atoms were introduced geometrically. Calculations were performed with SHELXTL-97 program package. Crystallographic data for the structures reported in this paper have been deposited with the Cambridge Crystallographic Data Centre as supplementary publication no. CCDC: 931717(for **2**), 938586(for **3**), 921209(for **4**), 928376(for **5**).

2.2. Optical measurements

The one-photon absorption (OPA) spectra were recorded on a SPECORD S600 spectrophotometer. The one-photon excited fluorescence spectra measurements were performed using a Hitachi F-7000 fluorescence spectrophotometer. In the

measurements of emission and excitation spectra, the pass width is 5 nm for all compounds. OPA and OPEF of compounds **1–6** were measured in five organic solvents of different polarities with the concentration of 1.0×10^{-5} mol L⁻¹. The quartz cuvettes used are of 1 cm path length. The absolute fluorescence quantum yield (Φ) values were determined using an integrating sphere. For time-resolved fluorescence measurements, the fluorescence signals were collimated and focused onto the entrance slit of a monochromator with the output plane equipped with a photomultiplier tube (HORIBA HuoroMax-4P). The decays were analyzed by ‘least-squares’. The quality of the exponential fits was evaluated by the goodness of fit (χ^2).

Two-photon absorption cross-sections (δ) of the samples were obtained by two-photon excited fluorescence method [26] at femtosecond laser pulse and Ti:sapphire system (680–1080 nm, 80 MHz, 140 fs) as the light source. The sample was dissolved in different solvents at a concentration of 5.0×10^{-4} mol L⁻¹. The intensities of TPEF spectra of the reference and the sample were determined at their excitation wavelength. Thus, TPA cross-section of samples was determined by Eq.:

$$\delta = \delta_{ref} \frac{\Phi_{ref} c_{ref} n_{ref} F}{\Phi c n F_{ref}}$$

Where the *ref* subscripts stand for the reference molecule (here fluorescein in the aqueous NaOH solution (1 mol L⁻¹) at concentration of 1.0×10^{-3} mol L⁻¹ was used as reference). δ is the TPA cross-sectional value, c is the concentration of the solution, n is the refractive index of the solution, F is the TPEF integral intensities

of the solution emitted at the exciting wavelength, and Φ is the fluorescence quantum yield. The δ_{ref} value of reference was taken from the literature [27].

2.3. Cytotoxicity assays in cells

To ascertain the cytotoxic effect of the compounds, the 3-(4,5-dimethylthiazol-2-yl)-2,5-diphenyltetrazolium bromide (MTT) assay was performed. HepG2 cells were trypsinized and plated to ~70% confluence in 96-well plates 24 h before treatment. Prior to the compounds' treatment, the DMEM was removed and replaced with fresh DMEM, and aliquots of the compound stock solutions (1 mM DMSO) were added to obtain final concentrations of 5, 10, 20 and 40 μM . The treated cells were incubated for 24 h at 37 °C and under 5% CO_2 . Subsequently, the cells were treated with 5 mg/mL MTT (40 μL /well) and incubated for an additional 4 h (37 °C, 5% CO_2). Then, DMEM was removed, the formazan crystals were dissolved in DMSO (150 μL /well), and the absorbance at 490 nm was recorded. The cell viability (%) was calculated according to the following equation: cell viability % = $\text{OD}_{490}(\text{sample})/\text{OD}_{490}(\text{control}) \times 100$, where $\text{OD}_{490}(\text{sample})$ represents the optical density of the wells treated with various concentration of the compounds and $\text{OD}_{490}(\text{control})$ represents that of the wells treated with DMEM + 10% FCS. Three independent trials were conducted, and the averages and standard deviations are reported. The reported percent cell survival values are relative to untreated control cells.

2.4. Cell culture and incubation

HepG2 cells were seeded in 6 well plates at a density of 2×10^5 cells per well and grown for 96 hours. The cell cultures were incubated with the dyes (10% PBS: 90% cell media) at concentrations 2.5 μ M and maintained at 37 °C in an atmosphere of 5% CO₂ and 95% air for incubation times ranging for 2 hours. The cells were then washed with PBS (3 \times 3 mL per well) and 3 mL of PBS was added to each well.

2.5. Fluorescence imaging

HepG2 cells were luminescently imaged on a Zeiss LSM 710 META upright confocal laser scanning microscope using magnification 40 \times and 100 \times water-dipping lenses for monolayer cultures. Image data acquisition and processing was performed using Zeiss LSM Image Browser, Zeiss LSM Image Expert and Image J.

2.6. Synthesis

6-phenyl-4'-(4-[4-(1H-imidazolyl)styryl]phenyl)-2, 2'-bipyridine (**1**). All compounds were prepared by a similar procedure. 4-(6-Phenyl-2, 2'-bipyridine-4')-benzyl triphenyl phosphonium bromide (E) (6.63 g, 10 mmol), 4-(1H-imidazol-1-yl)benzaldehyde (1.72 g, 10 mmol) and *t*-BuOK (5.60 g, 50 mmol) were placed in a dry mortar. The mixture milled vigorously for about 20 min. It became sticky, and then tetrahydrofuran (5 mL) was added. It was continuously milled for 10 min. After completion of the reaction (monitored by Thin Layer Chromatography (TLC)), the mixture was poured into distilled water

(500 mL). The product was extracted twice with CH_2Cl_2 , and the organic layer was dried overnight over anhydrous MgSO_4 . The solvent was removed with a rotary evaporator to give the crude product. It was purified by recrystallization from the mixture of CH_2Cl_2 and methanol. Yield: 80%. mp: 268.8 °C. Anal. Calcd. (%) for $\text{C}_{33}\text{H}_{24}\text{N}_4$: C, 83.17; H, 5.08; N, 11.76. Found (%): C, 83.51; H, 4.75; N, 11.50. FT-IR (KBr, cm^{-1}): 3131, 3033, 1600, 1583, 1565, 1523, 1476, 1390, 1302, 1258, 1112, 1050, 970, 833, 792, 730, 689, 539. ^1H NMR ($(\text{CD}_3)_2\text{SO}$, 400 MHz): δ 7.13 (s, 1H), 7.46 (s, 2H), 7.50-7.55 (m, 2H), 7.59 (t, $J = 8.4$ Hz, 2H), 7.72 (d, $J = 8.4$ Hz, 2H), 7.81-7.85 (m, 5H), 8.02-8.08 (m, 3H), 8.34-8.40 (m, 4H), 8.66 (t, $J = 5.6$ Hz, 2H), 8.78 (d, $J = 4.4$ Hz, 1H). ^{13}C NMR (100 MHz, CDCl_3): δ (ppm) = 117.2, 118.2, 121.6, 121.7, 123.9, 127.1, 127.3, 127.6, 127.7, 127.9, 127.8, 128.8, 129.2, 129.9, 136.3, 136.8, 137.0, 137.6, 138.2, 139.5, 149.0, 149.5, 156.3, 156.3, 157.3. MS (ESI) (m/z): Calc. for $\text{C}_{33}\text{H}_{24}\text{N}_4$: 477.20 $[\text{M}]^+$; Found: 477.21 $[\text{M}]^+$.

6-Phenyl-4'-(4-[4-(1H-1,2,4-triazolyl)styryl]phenyl)-2,2'-bipyridine (**2**). The reaction was carried out using the same method used for **1**, except that 4-(1H-1, 2, 4-triazol-1-yl)benzaldehyde (1.73 g, 10 mmol) was used instead of 4-(1H-imidazol-1-yl)benzaldehyde. Yield: 82%. mp: 266.5 °C. Anal. Calcd. (%) for $\text{C}_{32}\text{H}_{23}\text{N}_5$: C, 80.48; H, 4.85; N, 14.66. Found (%): C, 80.16; H, 4.49; N, 14.98. FT-IR (KBr, cm^{-1}): 3130, 3032, 1600, 1583, 1565, 1542, 1522, 1473, 1276, 1214, 1045, 976, 837, 792, 732, 690, 670, 539. ^1H NMR (CDCl_3 , 400 MHz): δ 7.21 (s, 2H), 7.36 (s, 1H), 7.47 (t, $J = 6.8$ Hz, 1H), 7.55 (t, $J = 7.2$ Hz, 2H), 7.66-7.70 (m, 6H), 7.86-7.91 (m, 3H), 8.01 (s, 1H), 8.13 (s, 1H), 8.22 (d, $J = 7.2$ Hz, 2H), 8.58

(s, 1H), 8.69, 8.73 (m, 3H). ^{13}C NMR (100 MHz, CDCl_3): δ (ppm) = 117.2, 118.2, 120.2, 121.7, 124.0, 127.1, 127.3, 127.6, 127.8, 127.9, 128.8, 129.2, 136.1, 137.2, 137.6, 138.1, 139.4, 140.7, 148.9, 149.5, 152.6, 156.2, 157.3. MS (ESI) (m/z): Calc. for $\text{C}_{32}\text{H}_{23}\text{N}_5$: 478.20 $[\text{M}]^+$; Found: 478.20 $[\text{M}]^+$.

6-Phenyl-4'-(4-[4-(1H-carbazolyl)styryl]phenyl)-2,2'-bipyridine (3). The reaction was carried out using the same method used for **1**, except that 4-(carbazol-9-yl)benzaldehyde (2.71 g, 10 mmol) was used instead of 4-(1H-imidazol-1-yl)benzaldehyde. Yield: 82%. mp: 172.6 °C. Anal. Calcd. (%) for $\text{C}_{42}\text{H}_{29}\text{N}_3$: C, 87.62; H, 5.08; N, 7.30. Found (%): C, 87.29; H, 5.39; N, 7.65. FT-IR (KBr, cm^{-1}): 3035, 1599, 1582, 1564, 1540, 1513, 1475, 1449, 1390, 1361, 1333, 1313, 1228, 1116, 969, 832, 791, 771, 746, 721, 689, 620, 537. ^1H NMR (CDCl_3 , 400 MHz): δ 6.73 (s, 2H), 7.25-7.28 (m, 1H), 7.36-7.52 (m, 15H), 7.80 (d, $J = 7.6$ Hz, 2H), 7.89 (t, $J = 6.4$ Hz, 1H), 7.99 (s, 1H), 8.12 (d, $J = 8.0$ Hz, 2H), 8.18 (d, $J = 7.2$ Hz, 2H), 8.69-8.74 (m, 3H). ^{13}C NMR (100 MHz, CDCl_3): δ (ppm) = 109.8, 117.6, 118.4, 120.0, 120.3, 122.0, 123.4, 124.0, 125.9, 126.7, 127.0, 127.2, 128.7, 129.2, 129.6, 130.1, 130.2, 130.3, 136.0, 136.6, 137.2, 138.0, 139.2, 140.6, 148.0, 149.7, 155.5, 157.3. MS (ESI) (m/z): Calc. for $\text{C}_{42}\text{H}_{29}\text{N}_3$: 576.24 $[\text{M}]^+$; Found: 576.24 $[\text{M}]^+$.

6-Phenyl-4'-(4-[(9-anthryl)vinyl]phenyl)-2, 2'-bipyridine (4). Compound **4** was prepared according to a similar procedure of **1** using 9-anthracene aldehyde (2.06 g, 10 mmol) instead of 4-(1H-imidazol-1-yl) benzaldehyde. Yield: 78%. mp: 207.8 °C. Anal. Calcd. (%) for $\text{C}_{38}\text{H}_{26}\text{N}_2$: C, 89.38; H, 5.13; N, 5.49. Found (%): C,

89.69; H, 4.78; N, 5.52. FT-IR (KBr, cm^{-1}): 3050, 2922, 1600, 1581, 1566, 1539, 1513, 1469, 1449, 1412, 1389, 896, 879, 837, 793, 777, 735, 693, 638, 614, 520. ^1H NMR (CDCl_3 , 400 MHz): δ 7.04 (d, $J = 16.4$ Hz, 1H), 7.40 (s, 1H), 7.50-7.51 (m, 5H), 7.56 (t, $J = 7.2$ Hz, 2H), 7.83 (d, $J = 7.2$ Hz, 2H), 7.91 (d, $J = 7.2$ Hz, 1H), 7.96 (d, $J = 7.6$ Hz, 2H), 8.03-8.07 (m, 4H), 8.24 (d, $J = 7.6$ Hz, 2H), 8.38-8.40 (m, 2H), 8.44 (s, 1H), 8.26 (s, 1H), 8.76 (s, 2H). ^{13}C NMR (100 MHz, CDCl_3): δ (ppm) = 125.2, 125.4, 125.6, 125.7, 125.8, 126.0, 126.7, 127.1, 127.3, 127.6, 128.0, 128.1, 128.7, 128.9, 129.0, 129.7, 130.0, 131.5, 133.4, 134.3, 135.0, 136.5, 137.9, 138.4, 141.6. MALDI-TOF MS Calc for $\text{C}_{38}\text{H}_{26}\text{N}_2$, 510.21; Found, 510.50.

6-Phenyl-4'-(4-[4-(diphenylamino)styryl]phenyl)-2, 2'-bipyridine (5). Compound **5** was prepared according to a similar procedure of **1** using 4-diphenylamino benzaldehyde (2.73 g, 10 mmol) instead of 4-(1H-imidazol-1-yl) benzaldehyde. Yield: 75%. mp: 182.0 °C. Anal. Calcd. (%) for $\text{C}_{42}\text{H}_{31}\text{N}_3$: C, 87.32; H, 5.41; N, 7.27. Found (%): C, 87.68; H, 5.15; N, 7.05. FT-IR (KBr, cm^{-1}): 3030, 2955, 2923, 1585, 1513, 1489, 1465, 1378, 1329, 1313, 1275, 1173, 1023, 969, 834, 753, 734, 694, 617, 537, 502. ^1H NMR ($(\text{CD}_3)_2\text{SO}$, 400 MHz) δ (ppm): 6.98 (d, $J = 8.0$ Hz, 2H), 7.03-7.10 (m, $J = 7.3$ Hz, 6H), 7.24 (d, $J = 16.4$ Hz, 1H), 7.30-7.38 (m, $J = 8.4$ Hz, 5H), 7.49-7.60 (m, $J = 6.0$ Hz, 6H), 7.78 (d, $J = 8.0$ Hz, 2H), 8.03 (d, $J = 7.2$ Hz, 3H), 8.38 (t, $J = 9.6$ Hz, 3H), 8.65 (d, $J = 11.2$ Hz, 2H), 8.77 (d, $J = 4.8$ Hz, 1H). ^{13}C NMR (100 MHz, CDCl_3): δ (ppm) = 117.2, 118.2, 121.6, 123.1, 123.4, 123.9, 124.6, 126.1, 126.9, 127.1, 127.5, 128.8, 129.1, 129.1, 129.3, 131.2,

137.1, 137.2, 138.5, 139.5, 147.5, 147.6, 148.9, 149.7, 156.2, 157.2. MALDI-TOF MS Calc for C₄₂H₃₁N₃, 577.25; Found, 577.36.

6-Phenyl-4'-(4-[4-(4,4'-diethoxyphenyl)amino]styryl)phenyl)-2,2'-bipyridine (6).

Compound **6** was prepared according to a similar procedure of **1** using 4-[(4,4'-diethoxyphenyl)amino]benzaldehyde (3.61 g, 10 mmol) instead of 4-(1H-imidazol-1-yl)benzaldehyde. Yield: 69%. mp: 153.8 °C. Anal. Calcd. (%) for C₄₆H₃₉N₃O₂: C, 82.98; H, 5.90; N, 6.31. Found (%): C, 82.65; H, 5.69; N, 6.68. FT-IR (KBr, cm⁻¹): 3031, 2976, 2925, 1590, 1502, 1474, 1389, 1319, 1281, 1236, 1165, 1111, 1044, 961, 826, 794, 692, 579, 530. ¹H NMR (CDCl₃, 400 MHz): δ 1.42 (t, *J* = 7.0 Hz, 6H), 4.00-4.05 (q, *J* = 7.0 Hz, 4H), 6.84 (d, *J* = 7.2 Hz, 4H), 6.92 (d, *J* = 8.4 Hz, 2H), 6.98 (d, *J* = 16.4 Hz, 1H), 7.07 (d, *J* = 9.2 Hz, 4H), 7.14 (d, *J* = 16.4 Hz, 1H), 7.35 (d, *J* = 8.4 Hz, 2H), 7.51-7.58 (m, 3H), 7.67 (d, *J* = 7.2 Hz, 2H), 7.90 (s, 1H), 8.10 (d, *J* = 6.8 Hz, 2H), 8.18 (s, 3H), 8.51 (s, 1H), 9.02-9.07 (m, 2H), 9.41 (s, 1H). ¹³C NMR (100 MHz, (CD₃)₂SO): δ (ppm) = 16.5, 63.1, 115.4, 116.0, 117.6, 118.8, 120.8, 124.4, 124.5, 126.8, 126.8, 127.0, 127.3, 127.6, 128.5, 128.7, 129.3, 135.7, 138.5, 138.7, 139.6, 148.2, 148.9, 149.2, 155.2, 155.6, 156.4. MALDI-TOF MS Calc for C₄₆H₃₉N₃O₂, 665.30; Found, 665.01.

3. Results and discussion

3.1 Synthesis

Scheme 1

Synthetic routes of compounds **1-6** are depicted in Scheme 1. The syntheses of intermediates were described in the Supporting Information, and all kinds of substituted benzaldehydes, namely, 4-(1H-imidazol-1-yl)benzaldehyde, 4-(1H-1,2,4-triazol-1-yl)benzaldehyde, 4-(carbazol-9-yl)benzaldehyde, 4-diphenylaminobenzaldehyde, and 4-[(4,4'-diethoxyphenyl)amino]benzaldehyde were prepared according to the literature procedures [28,29]. Substituted benzaldehydes and 4-(6-phenyl-2,2'-bipyridine-4')benzyl triphenyl phosphonium bromide were coupled by the solvent free Wittig reaction, compounds **1-6** were obtained in high yields. All compounds exhibit a simple preparation and purification at lower cost. In our experiments, we ground the reaction mixture in a mortar, using *t*-BuOK as base. The reaction could be accomplished within half an hour and the product could be handled easily and the yield was above 70%. Therefore, solvent free Wittig reaction is an inexpensive and convenient method to synthesize alkene. Single crystals of **2-5** were obtained by slow evaporation from methanol/CH₂Cl₂ mixture solution.

3.2. Crystal structures

Fig. 1

The structures of compounds **2-5** were confirmed by X-ray crystallography. The molecular structures have been depicted in Fig. 2–5a. The structural features

are discussed from the following three aspects. First, in the electronic acceptor moiety, as shown in Fig. 1 and Table S2, the P0 ring adjoins the P1, P2, and P3 rings with the dihedral angles being 8.78/8.10, 8.45/8.69, and 27.12/28.01° for **2**, 1.55, 2.35, and 24.59° for **3**, 7.22, 9.63, and 27.90° for **4**, as well as 6.27, 13.19, and 32.42° for **5**. These angles indicate that the acceptor moieties are all good planar, meaning there exist good π -conjugated system in the electronic acceptor moieties of compounds **2-5**. Second, at the electronic donor moiety, the smaller dihedral angle (1.34°) between P4 and P5 in **2** indicates the higher π -conjugated degree. However, the dihedral angles between the carbazolyl ring (P5) and its neighboring phenyl plane P4 in **3**, as well as the anthryl ring and P3 in **4** are 62.47 and 62.16°, respectively, indicating the highly twisted conformations. This highly twisted conformation will reduce the degree of π conjugation, and further decrease the charge transfer from donor to acceptor. For **5**, at the triphenylamine moiety, three phenyl rings around the central nitrogen are arrayed in a propeller-like fashion and they are twisted from the trigonal NC₃ plane with the torsion angles of 45.94, 34.68 and 42.85°, respectively. The N atom in the triphenylamine group has an sp² geometry favoring intramolecular p- π interactions between nitrogen and its adjacent phenyl rings. Third, in the conjugated bridge section, as shown in Tables S2, S3, the linkage between P3 and P4 is fine π -conjugated, and the bond lengths of the C–C bonds between P3 and P4 in **2-5** are in the range of 1.264(7) and 1.53(1) Å. And other linkage bond lengths between two neighboring aromatic rings are all quite conjugated and are shorter than the normal C–C single bond

(1.54 Å) or C–N single bond (1.47 Å). It is worth noting that, for **5**, the dihedral angle between P3 and P4 is only 9.33°, and it is much smaller than those in **3** and **4** (18.36° and 62.16°, respectively). The result clearly shows the more planar structure of **5**, which is expected to facilitate TPA.

Fig. 2

In short, the structural features suggest that all non-hydrogen atoms of molecules **2-5** show different conjugate degree, which combined with the different electron-donating strength of terminal moieties will exert very important influence on the fluorescence properties.

Fig. 3

The molecules are held together in the crystal by the weak C–H⋯ π stacking and/or C–H⋯N hydrogen bonding interactions, and no π - π stacking interaction was found. As shown in Fig. 2b, the neighboring units of **2** are linked each other through C(5)–H(5)⋯N(4), C(5)–H(5)⋯N(4) hydrogen bonding and C(27)–H(27)⋯ π interactions to form one-dimensional structure along *a*-axis. As shown in Fig. 3-5b, in the structures of **3-5**, only C–H⋯ π interactions were detected, and the weak interactions link the molecules to generate one-dimensional (for **4** and **5**) or two-dimensional (for **3**) structures.

Fig. 4

Fig. 5

3.3 TDDFT calculations

To further investigate the influence of different electron donors on the characteristic of charge transition of the compounds, the quantum chemical calculations based on time-dependent density functional theory (TDDFT) were performed on **1-6** using Gaussian 03 program. The B3LYP/6-31G basis sets were used for the calculations. The TDDFT calculations were performed on the optimized structure. The isosurfaces of the highest occupied and the lowest unoccupied molecular orbitals (HOMO and LUMO) are shown in Fig. 6. For **1** and **2**, the electron-cloud is delocalized throughout the entire backbones, and the HOMO and LUMO diagrams clearly show the π - π^* transitions characteristics upon photoexcitation. This result suggests that, on the one hand, the optical transition from LUMO to HOMO is a direct one, which offers a high fluorescent efficiency, on the other hand, the molecules have no intramolecular charge transfer (ICT) process. In sharp contrast, with the enhancement of the electron-donating ability, the HOMO and LUMO of **3-6** exhibit the obvious intramolecular charge transfer characteristics, which may be favorable for the TPA of the compounds.

Fig. 6

3.4. One-photon absorption and emission properties

The one-photon absorption and one-photon excited fluorescence were measured in five solvents of different polarities at the concentration of 1×10^{-5} mol/L. There is no linear absorption beyond 450 nm for the molecules. The linear and nonlinear optical properties for **1-6** in different polar solvents are listed in

Table 1. In order to investigate the spectra relationship of the different compounds, the OPA and the OPEF data of **1–6** in ethyl acetate were just used as examples to discussed in detail. As expected, the absorption maxima of the compounds mainly depend on the nature of the different electron-donating edge substituents, and the linear absorption maxima for these dyes are tuned from 332 to 404 nm by using different electron donors.

Fig. 7

As shown in Fig. 7 and Fig. S21, S22, compounds **1**, **2** and **4** exhibit one absorption band. The absorption maxima are located at 337, 335 and 386 nm in ethyl acetate, respectively, which correspond to the π - π^* transitions of the backbones of **1** and **2**, as well as the intramolecular charge-transfer for **4** on the basis of density functional calculations [30]. The shoulder peak at 366 nm of **4** originates from a locally excited (LE) state of anthracene. Compounds **3**, **5** and **6** are featured by two distinct absorption bands. The bands in the high energy region are assigned to the π - π^* transition, and those at longer wavelengths originates from intramolecular charge-transfer interaction. In short, the red-shifted linear absorption maximum with the order of **2** < **1** < **3** < **5** < **6** is consistent with the trend of the increasing electron-donating ability and can be primarily explained by the significant stabilization of the LUMO leading to a smaller HOMO-LUMO energy gap [31].

Fig. 8

From Fig. 7, Table 1, and Fig. S21, S22, one can see that the linear absorption spectra of compounds **1-6** were slightly red-shifted with increasing solvent polarity (except in dichloromethane) and all of them show definite solvatochromic behavior. This positive solvatochromism is indicative of a larger stabilization of the excited state as compared to the ground state by a polar solvent, which suggests that a significant charge redistribution takes place upon excitation [22a].

Table 1

As shown in Fig. 7 and Fig. S20, S21, all of the compounds have strong one-photon fluorescence. The fluorescence spectra exhibit a single peak, which indicates that the emission occurs from the lowest excited state with the largest oscillator strength. Compounds **1-6** all have a trend of red-shift with increasing the solvent polarity (except in dichloromethane). Accompanying this bathochromic shift is a weakening of the emission intensity. The Stokes shifts also show a tendency to increase with increasing the solvent polarity. This can be explained by the fact that the excited state possess a higher polarity than the ground state, and the increased dipole–dipole interaction between the solute and solvent leads to a lowering of the energy level of the excited state [32]. Additionally, with increasing the solvent polarity, the red-shifts of **3**, **5** and **6** are more obvious than those of **1**, **2** and **4**, which may be due to the more strength of the donors in **3**, **5** and **6**, as well as different charge-transfer mechanism of them. It is noted that the one-photon fluorescence emission of **6** highly quenched in ethanol, acetonitrile and DMF, and

the same case occurs in the two-photon fluorescence emission, which may be due to the poor solubility of **6** in those solvents. As shown in Fig. 8, the maximum emission of **1-6** in ethyl acetate locates at 408, 403, 436, 488, 487 and 524 nm, respectively. The order of emission wavelength for dyes **1**, **2**, **3**, **5**, and **6** was consistent with the strength of the donors: (4,4'-diethoxyphenyl)amino > diphenylamine > carbazole > imidazole > triazole. The emission wavelengths for **3-6** are much longer than those for **1** and **2**, which can be explained by the fact that the donor groups in **3-6** have stronger electron-donating strength than the imidazolyl and triazolyl groups. Correspondingly, the charge transfer within the molecules of **3-6** is much stronger and the band gaps are smaller, which can be confirmed by the DFT calculation [33]. Although the electron donating ability of carbazolyl is stronger than that of anthryl, the emission band of dye **4** is red-shift about 52 nm compared to that of **3**, which may be explained that the shorter conjugation bridge of **4** enhances the intramolecular charge-transfer interaction.

The fluorescence quantum yield values were determined using an integrating sphere. As shown in Table 1, all the compounds have high fluorescence quantum yields, proving the validity of our molecular design strategy for fluorescence-based solution application. The fluorescence quantum yields of **1** and **2** are similar in the same solvent, which may be due to the similar structure character of the molecules. Compared with the others, **4** shows the lower fluorescence quantum yield, which might be caused by its twisted structure. Molecules with a large torsional distortion in the ground state go through fast

nonradiative decay and show small fluorescence quantum yield. The fluorescence quantum yield of **6** is slightly lower than that of **5**, which suggests that a significant non-radiative transition might occur in **6** due to its flexible (4,4'-diethoxyphenyl)amino chains [34]. The same result was obtained in our previous work [35]. Therefore, we draw a conclusion that the compounds with diphenylamine as the donor moiety appear to have high fluorescence quantum yield compared with the dyes with (4,4'-diethoxyphenyl)amino as the donor moiety. Additionally, concurrently with the spectral red-shift and intensity reduction, the fluorescence quantum yields of all compounds are gradually reduced with increasing solvent polarity.

To further characterize the photophysical properties of the synthesized compounds, time-resolved fluorescence measurements were performed by using the single-photon-counting method with picosecond laser excitation. The fluorescence lifetimes (τ) of compounds **1-6** in ethyl acetate are 0.89 ns, 0.82 ns, 1.38 ns, 2.68, 1.84 ns and 2.97 ns, respectively (Table 1 and Fig. 9). The result further indicates that introducing strong electronic donor group may greatly increase the ICT strength and reduce the energy of the excited state. Furthermore, the fluorescence lifetimes almost show a tendency to increase with increasing polarity of the solvents.

Fig. 9

Additionally, the fluorescence lifetimes of **1-6** in solution was calculated by multiplying the corresponding quantum yield on natural lifetime, which can be

easily calculated from the known Strickler-Berg equation (eqn. (1)) [36].

(1)

in which n is the refractive index, I is the fluorescence emission, ϵ is the extinction coefficient, and $\tilde{\nu}$ is the wave-number. The natural radiative lifetime τ_0 and the fluorescence lifetime τ are related through the quantum yield Φ by

(2)

The calculated fluorescence lifetimes are showed in Table 1, which also show a tendency to increase with increasing polarity of the solvents, according with the experimental values.

As discussed above, the fluorescence spectra show large Stokes shifts depending on the solvent polarity. The Lippert-Mataga equation is the most widely used equation to evaluate the dipole moment changes of the compounds with photoexcitation [37]:

(1)

(2)

in which $\Delta\nu = \nu_{\text{abs}} - \nu_{\text{em}}$ stands for Stokes shift, ν_{abs} and ν_{em} are absorption and emission (cm^{-1}), \hbar is the Planck's constant, c is the velocity of light in vacuum, a is the Onsager radius and b is a constant. Δf is the orientation polarizability, μ_e and μ_g are the dipole moments of the emissive and ground states, respectively, and ϵ_0 is the permittivity of the vacuum. $(\mu_e - \mu_g)^2$ is proportional to the slope of the Lippert

-Mataga plot.

Fig. 10

As shown in Fig. 10, the Lippert-Mataga plots of compounds **3** and **5** give much larger slope than those of other dyes, which indicates larger dipole moment changes for **3** and **5** with photoexcitation [37]. The slope of the best-fit line is related to the dipole moment change between the ground and excited states ($\mu_e - \mu_g$). The slopes of the lines are 6547, 3771, 10721, 3228 and 11604 cm^{-1} for compounds **1-5**, respectively. So the values of $\mu_e - \mu_g$ were calculated as 12.6 D for **1**, 8.4 D for **2**, 17.0 D for **3**, 8.9 D for **4**, and 17.5 D for **5**. The large values of **3** and **5** indicate that the molecule in the excited state has an extremely polar structure, which is the typical characterization of ICT [38]. The result accords with their linear and nonlinear optical properties.

3.5. Two-photon excited fluorescence spectra and TPA cross-sections

The detail experiments indicate that compounds **5** and **6** show strong two-photon excited fluorescence, and the fluorescence spectra data are listed in Table 1. However, **3** only exhibits very weak TPEF (Fig. S28), and **1**, **2** as well as **4** show no TPEF. This fact clearly showed that careful selection of the electron-donating group can have a significant impact on the TPEF behavior of dyes. They have no linear absorption beyond 450 nm, which indicates that there are no energy levels corresponding to an electron transition in this spectral range. Therefore, if frequency upconverted fluorescence appears upon excitation with a

tunable laser in this spectral range, it should be attributed to multi-photon absorption excited fluorescence. Because of very weak TPEF of **3**, here, only two-photon excited fluorescence of **5** and **6** are discussed in detail. Two-photon fluorescence spectra of compounds **5** and **6** in ethyl acetate pumped by femtosecond laser pulses at 300 mW at different excitation wavelengths are presented in Fig. 11. The insert figures show TPF spectra under different pump intensities and logarithmic plots of the fluorescence integral versus pumped powers with a slope of 1.95 for **5** and 1.92 for **6** when the input laser power is increasing, suggesting a two-photon excitation mechanism. As shown in Fig. 11, and Fig. S25-S27, compounds **5** and **6** display good TPA activity in the range of 680-900 and 680-960 nm, respectively, and the optimal excitation wavelengths are 800 and 820 nm, respectively, which are slightly higher than twice the corresponding linear absorption maximum (390 and 400 nm for **5** and **6**, respectively). From Table 1, one can see that the peak positions of TPEF show red shift compared to those of SPEF. This can be explained by the effect of reabsorption in the high concentration solution [39].

Fig. 11

From Fig. S29, we can clearly find that the maxima of the two-photon excited fluorescence also exhibits red-shift with increasing solvent polarity, and the TPEF emission of **6** highly quenched in ethanol, acetonitrile and DMF, which is similar to one-photon excited fluorescence. This observation indicates that both of the

one-photon excited fluorescence and two-photon excited fluorescence are produced from the same excited state even though two different excitation processes are used. Two-photon absorption cross-sections have been measured using TPEF. As shown in Table 1 and Fig. 12, the maximum absorption cross-sections are 1378 GM for **5** and 1654 GM for **6**. Obviously, the result indicates that the TPA cross sections of the linear conjugated molecules with a D- π -A structure strongly depend on the electron donating ability of the donor moiety and the coplanarity of backbone. A stronger donor as well as good planarity of backbone will generally increase charge transfer and enhance the transition dipole moments, contributing to a larger value of δ_{TPA} because of stronger ICT processes [40].

Fig. 12

3.6. Cytotoxicity assays

Cytotoxicity is a potential side effect of dyes that must be controlled when dealing with living cells or tissues. Considering their application in cell imaging, the MTT assay was performed to ascertain the cytotoxic effect of compounds **1-6** against HepG2 cells over a period of 24 h. Fig. S30 shows the cell viability for HepG2 cells treated with **1-6** at different concentrations for 24 h. The results clearly indicated that HepG2 cells incubated with concentration of 5 μM of compounds **1-6** remained 89%, 88%, 80%, 70%, 89% and 86%, respectively viable after feeding time of 24 h, demonstrating the biocompatibility of all compounds. Additionally, it was found that

high concentration only leads to a gradual decrease of viable cells as shown in Fig. S31. As a result, cytotoxicity tests definitely indicate that the low-micromolar concentrations of compounds **1**, **2**, **5** and **6** have small toxic effects on living cells over a period of 24 h, and they have great potentials for further biological studies.

3.7. One- and two- photon fluorescence microscopy cell imaging

To further demonstrate the potential of the compounds in one- and two-photon fluorescence microscopy imaging applications in living cells, we carried out imaging studies with live HepG2 cells stained with compounds **1-6** by both one- and two-photon microscopy. In one-photon microscopy imaging, the excitation wavelength was fixed at 405 nm. As shown in Fig. 13, 14a, and Fig. S32-35a, bright blue fluorescence from the cells indicates that compounds **1-6** could be effectively internalized by HepG2 cells. In contrast, except for **4**, the images of HepG2 cells stained with other compounds show brighter fluorescence signal, which is due to the higher fluorescence quantum yields and stronger emission abilities of them. The bright-field image of each cell was taken immediately prior to the fluorescence microscopy imaging. The fluorescent images and the merged images confirmed that incubation with HepG2 cells for 2 hours (Fig. 13, 14, and Fig. S31-34), compounds **1-6** all went through the membrane and localized uniformly in the cytoplasm, suggesting that only the cell cytoplasm can be labelled by the dyes.

Fig. 13

Two-photon fluorescence microscopy provides key advantages over one-photon fluorescence imaging, namely, increased penetration depth, lower tissue autofluorescence and self-absorption, and reduced photodamage and photobleaching [41]. In two-photon microscopy imaging, the optimal excitation wavelength of each compound was used. As shown in Fig. 14b and Fig. S34b, the TPEF image of HepG2 cells shows bright green fluorescence upon excitation. These results highlight the potential of **5** and **6** for both one- and two-photon fluorescence microscopy imaging applications. The image of HepG2 cells stained with **3** shows weak fluorescence (Fig. S33b), which may be due to the weak fluorescence emission and smaller TPA cross-section of **3**.

Fig. 14

4. Conclusion

In conclusion, the fluorescence properties of compounds **1-6** were successfully tuned from OPEF to TPEF through increasing electron-pushing abilities of donors. As a result, compounds **5** and **6** exhibit two-photon excited fluorescence properties, due to the enhanced intramolecular charge transfer caused by the stronger electron donors and more planar structures. The corresponding fluorescence property, low toxicity on living cells, as well as cell permeability enable them to be very promising in one- or two-photon fluorescence cell imaging.

Acknowledgements

This work was supported by Program for New Century Excellent Talents in University (China), Doctoral Program Foundation of Ministry of Education of China (20113401110004), National Natural Science Foundation of China (21271003, 21271004, 21201005), the 211 Project of Anhui University, Doctoral Startup Foundation of Anhui University (33190077), the Anhui University Students Research Training Program (kyxl2012020), the Graduate Students Innovative Program of Anhui University (10117700063, 10117700066), Natural Science Foundation of Anhui Province (1308085QB33), and Natural Science Foundation of Education Committee of Anhui Province (KJ2012A024, KJ2013B201).

References

- [1] Morales AR, Frazer A, Woodward AW, White HYA, Fonari A, Belfield KD, et al. Design, synthesis, and structural and spectroscopic studies of push-pull two-photon absorbing chromophores with acceptor groups of varying strength. *J Org Chem* **2013**;78 (3):1014–25.
- [2] Marder SR, Gorman CB, Tiemann BG, Cheng LT. Stronger acceptors can diminish nonlinear optical response in simple donor-acceptor polyenes. *J Am Chem Soc* **1993**;115 (7):3006–7.
- [3] Pawlicki M, Collins HA, Denning RG, Anderson HL. Two-photon absorption and the design of two-photon dyes. *Angew Chem, Int Ed* **2009**;48 (18):3244–66.
- [4] Terenziani F, Katan C, Badaeva E, Tretiak, S, Desce MB. Enhanced two-photon absorption of organic chromophores: theoretical and experimental assessments. *Adv Mater* **2008**;20 (24):4641–78.

- [5] Guo EQ, Ren PH, Zhang YL, Zhang HC, Yang WJ. Diphenylamine end-capped 1, 4-diketo-3, 6-diphenylpyrrolo [3, 4-c] pyrrole (DPP) derivatives with large two-photon absorption cross-sections and strong two-photon excitation red fluorescence. *Chem Commun* **2009**;5859–61.
- [6] Gu M, Tannous T, Sheppard C. Three-dimensional confocal fluorescence imaging under ultrashort pulse illumination. *Opt Commun* **1995**;117 (5-6):406–12.
- [7] Dvornikov A, Walker E, Rentzepis P. Two-photon three-dimensional optical storage memory. *J Phys Chem A* **2009**;113 (49):13633–44.
- [8] Tian H, Feng Y. Next step of photochromic switches? *J Mater Chem* **2008**;18:1617–22.
- [9] Barsu C, Cheaib R, Chambert S, Queneau Y, Maury O, Cottet D, et al. Neutral push-pull chromophores for nonlinear optical imaging of cell membranes. *Org Biomol Chem* **2010**;8 (1):142–50.
- [10] Prasad PN, Reinhardt BA. Is there a role for organic materials chemistry in nonlinear optics and photonics? *Chem Mater* **1990**;2 (6):660–9.
- [11] He GS, Yuan L, Cheng N, Bhawalkar JD, Prasad PN. Nonlinear optical properties of a new chromophore. *J Opt Soc Am. B* **1997**;14 (5):1079–87.
- [12] Stryland EV, Wu YY, Hagan DJ, Soileau M, Mansour K. Optical limiting with semiconductors. *J Opt Soc Am B* **1988**;5 (9):1980–8.
- [13] Liu X, Sun YM, Zhang YH, Miao F, Wang GC, Wong WY, Et al. A 2, 7-carbazole-based dicationic salt for fluorescence detection of nucleic acids and two-photon fluorescence imaging of RNA in nucleoli and cytoplasm. *Org Biomol Chem* **2011**;9:3615–8.

- [14] Denk W, Strickler JH, Webb WW. Two-photon laser scanning fluorescence microscopy. *Science* **1990**;248 (4951):73–6.
- [15] Chung SJ, Zheng SJ, Odani T, Beverina L, Fu J, Marder SR, et al. Extended squaraine dyes with large two-photon absorption cross-sections. *J Am Chem. Soc* **2006**;128 (45):14444–5.
- [16] Pond SJK, Rumi M, Levin MD, Parker TC, Beljonne D, Marder SR, et al. One-and two-photon spectroscopy of donor-acceptor-donor distyrylbenzene derivatives: effect of cyano substitution and distortion from planarity. *J Phys Chem A* **2002**;106 (47):11470–80.
- [17] Rumi M, Ehrlich JE, Heikal AA, Perry JW, Barlow S, Marder SR, et al. Structure-property relationships for two-photon absorbing chromophores: bis-donor diphenylpolyene and bis (styryl) benzene derivatives. *J Am Chem Soc* **2000**;122 (39):9500–10.
- [18] Rumi, M. Pond SJK, Friedrichsen TM, Zhang Q, Bishop M, Zhang YD, Marder SR, et al. Tetrastylarene derivatives: comparison of one- and two-photon spectroscopic properties with distylarene analogues. *J Phys Chem C* **2008**;112 (21):8061–71.
- [19] Patra A, Pan M, Friend CS, Lin TC, Cartwright AN, Prasad PN, Electroluminescence properties of systematically derivatized organic chromophores containing electron donor and acceptor groups. *Chem Mater* **2002**;14 (10):4044–8.
- [20] Kannan R, He GS, Yuan LX, Xu FM, Prasad PN, Dombroskie AG, et al. Diphenylaminofluorene-based two-photon-absorbing chromophores with various π -electron acceptors. *Chem Mater* **2001**;13 (5):1896–904.
- [21] (a) Belfield KD, Liu Y, Negres RA, Fan M, Pan G, Hagan DJ, Hernandez FE, Two-photon photochromism of an organic material for holographic recording. *Chem Mater* **2002**;14 (9):3663–7; (b) Woo, H. Y. Hong JW, Liu B, Mikhailovsky A, Korystov D, Bazan GC.

- Water-soluble paracyclophane chromophores with large two-photon action cross sections. *J Am Chem Soc* **2005**;127 (3):820–1.
- [22] (a) Cooke MW, Hanan GS. Luminescent polynuclear assemblies. *Chem Soc Rev* **2007**;36:1466–76; (b) Eryazici I, Moorefield CN, Newkome GR. Square-planar Pd (II), Pt (II), and Au(III) terpyridine complexes: their syntheses, physical properties, supramolecular constructs, and biomedical activities. *Chem Rev* **2008**;108 (6):1834–95.
- [23] (a) Gao YH, Wu JY, Zhou H P, Yang JX, Zhang SY, Tian YP. et al. A sulfur-terminal Zn (II) complex and its two-photon microscopy biological imaging application. *J Am Chem Soc* **2009**;131 (14):5208–13; (b) Tian YP, Li L, Zhang JZ, Yang JX, Zhou HP, Wu JY, et al. Investigations and facile synthesis of a series of novel multi-functional two-photon absorption materials. *J Mater Chem* **2007**;17 (34):3646–54; (c) Zhou HP, Wang JQ, Zhou FX, Yang JX, Wu JY, Tian YP, et al. New five-coordinated mercury (II) dyes based on a novel 2,2':6',2''-terpyridine ligand: Structures, photophysical properties and DFT calculations to evaluate the halogen effect on the two-photon absorption. *Dyes Pigm* **2012**;95 (3):723–31; (d) Zhou HP, Zhou FX, Zheng Z, Yu ZP, Wu JY, Tian YP, et al. Three new five-coordinated mercury (II) dyes: Structure and enhanced two-photon absorption. *Dyes Pigm* **2011**;91(2):237-47; (e) Xu DL, Yu ZP, Yang MD, Wu JY, Tian YP, Zhou HP, et al. 2,2'-Bipyridine derivatives containing aza-crown ether: Structure, two-photon absorption and bioimaging. *Dyes Pigm* **2014**;100 (1):142–9.
- [24] (a) Biswas S, Wang XH, Morales AR, Ahn HY, Belfield KD. Integrin-targeting block copolymer probes for two-photon fluorescence bioimaging. *Biomacromolecules* **2011**;12 (2):441–9; (b) Wang XH, Nguyen DM, Yanez CO, Rodriguez L, Ahn HY, Belfield KD, et al.

- High-fidelity hydrophilic probe for two-photon fluorescence lysosomal imaging. *J Am Chem Soc* **2010**;132 (35):12237–9.
- [25] (a) Robson KCD, Spornova B, Koivisto BD, Schott E, Douglas G. Brown DG, Berlinguette CP. Systematic modulation of a bichromic cyclometalated ruthenium(II) scaffold bearing a redox-active triphenylamine constituent *Inorg Chem* **2011**;50 (13):6019–6028; (b) Muise SSR, Severin, HA, Koivisto BD, Robson KCD, Eduardo Schott E, Curtis P. Berlinguette CP. Regioselective C–H activation of cyclometalated bis-tridentate ruthenium complexes. *Organometallics* **2011**;30 (24):6628–6635; (c) Lazzaro DP, Phillip E. Fanwick PE, McMillin DR. Arylated versus cyclometalated platinum(II) polypyridines: photoluminescence from Pt(4'-R-tpy)Ph⁺ systems (R = NMe₂, N-Pyrrolidinyl, or 1-Pyrenyl). *Inorg Chem* **2012**;51 (20):10474–10476.
- [26] Lee SK, Yang WJ, Choi JJ, Kim CH, Jeon SJ, Cho BR. 2, 6-Bis [4-(p-dihexylaminostyryl) styryl] anthracene derivatives with large two-photon cross sections. *Org Lett* **2005**;7 (2):323–6.
- [27] Xu C, Webb WW. Measurement of two-photon excitation cross sections of molecular fluorophores with data from 690 to 1050 nm. *J Opt Soc Am B* **1996**;13 (3):481–91.
- [28] Zuo JL, Yang JX, Wan FZ, Tian YP, Tao XT, Jiang MH, et al. 2,6-Diphenylpyridine-based organic emitter for electroluminescent device. *J Photochem Photobiol A* **2008**;199 (2):322–9.
- [29] Zheng Z, Yu ZP, Yang MD, Jin F, Zhou HP, Tian YP, et al. Substituent group variations directing the molecular packing, electronic structure, and aggregation-induced emission property of isophorone derivatives. *J Org Chem* **2013**;78 (7):3222–34.
- [30] Stott TL, Wolf MO. Spectroscopic study of phosphine-substituted oligothiophenes. *J Phys Chem B* **2004**;108 (49):188815–9.

- [31] Zheng QD, He GS, Prasad PN. Novel two-photon-absorbing, 1, 10-phenanthroline-containing π -conjugated chromophores and their nickel (II) chelated complexes with quenched emissions. *J Mater Chem* **2005**;15:579–87.
- [32] Zheng Z, Zhang Q, Yu ZP, Yang MD, Zhou HP, Wu JY, Tian YP. Four new two-photon absorbing imidazo [4, 5-f] 1, 10-phenanthroline dye derivatives with different dipole moment orientation based on different groups: synthesis, optical characterization and bioimaging. *J Mater Chem C* **2013**;1:822–30.
- [33] Yang WJ, Kim DY, Kim CH, Jeong MY, Lee SK, Jeon SJ, et al. Triphenylamine derivatives with large two-photon cross-sections. *Org Lett* **2004**;6 (9):1389–92.
- [34] Zheng QD, He GS, Lin TC, Prasad PN. Synthesis and properties of substituted (p-aminostyryl)-1-(3-sulfooxypropyl) pyridinium inner salts as a new class of two-photon pumped lasing dyes. *J Mater Chem* **2003**;13:2499-504.
- [35] Zhou HP, Zheng Z, Xu GY, Kong L, Wu JY, Tian YP, et al. 1, 3, 5-Triazine-cored derivatives dyes containing triphenylamine based two-photon absorption: Synthesis, optical characterization and bioimaging. *Dyes Pigm* **2012**;94 (3):570–82.
- [36] Strickler S, Berg RA. Relationship between absorption intensity and fluorescence lifetime of molecules. *J Chem Phys* **1962**;37 (4):814–22.
- [37] Ji SM, Yang J, Yang Q, Liu SS, Chen MD, Zhao JZ. Tuning the intramolecular charge transfer of alkynylpyrenes: effect on photophysical properties and its application in design of OFF–ON fluorescent thiol probes. *J Org Chem* **2009**;74 (13):4855–65.
- [38] Irie M, Sayo K. Solvent effects on the photochromic reactions of diarylethene derivatives. *J Phys Chem* **1992**;96 (19):7671–4.

- [39] Xu F, Wang Z, Gong Q. Synthesis, characterization, and optical properties of two-photon-absorbing octupolar molecule with an s-triazine core. *Opt Mater* **2007**;29(6):723–7.
- [40] Nguyen DM, Frazer A, Rodriguez L, Belfield KD. Selective fluorescence sensing of zinc and mercury ions with hydrophilic 1, 2, 3-triazolyl fluorene probes. *Chem Mater* **2010**;22(11):3472–81.
- [41] Li L, Ge J, Wu H, Xu QH, Yao SQ. Organelle-Specific Detection of Phosphatase Activities with Two-Photon Fluorogenic Probes in Cells and Tissues. *J Am Chem Soc* **2012**;134(29):12157–67.

Figure captions

Fig. 1 The molecular structure labelling the dihedral angles between the neighboring aromatic rings.

Fig. 2 (a) The molecular structure of **2**. (b) The one-dimensional structure of **2** showing the C–H··· π stacking and C–H···N hydrogen bonding interactions. The dotted lines represent the weak interactions. Hydrogen atoms not participating in hydrogen bonding are omitted for clarity.

Fig. 3 (a) The molecular structure of **3**. (b) The two-dimensional structure of **3** showing the C–H··· π stacking. The dotted lines represent the weak interactions. Hydrogen atoms not participating in hydrogen bonding are omitted for clarity.

Fig. 4 (a) The molecular structure of **4**. (b) The one-dimensional structure of **4** showing the C–H··· π stacking. The dotted lines represent the weak interactions. Hydrogen atoms not participating in hydrogen bonding are omitted for clarity.

Fig. 5 (a) The molecular structure of **5**. (b) The one-dimensional structure of **5** showing the C–H··· π stacking. The dotted lines represent the weak interactions. Hydrogen atoms not participating in hydrogen bonding are omitted for clarity.

Fig. 6 The electron cloud distribution of frontier molecular orbitals of compounds **1–6**.

Fig. 7 Linear absorption and emission spectra of compounds **1** (a) and **5** (b) in five organic solvents.

Fig. 8 Normalized OPEF spectra of compounds **1–6** in ethyl acetate.

Fig. 9 Time-resolved fluorescence curves of **1–6** in ethyl acetate.

Fig. 10 Lippert-Mataga plots for compounds **1–5**.

Fig. 11 The TPEF spectra of **5** (a) and **6** (b) in ethyl acetate pumped by femtosecond laser pulses at 300 mW under the different excitation wavelengths. Insert figure: Output fluorescence (I_{out}) vs. the square of input laser power (I_{in}) under the optimal excitation wavelength at 800 nm for **5** and 820 nm for **6**, with $c = 5.0 \times 10^{-4} \text{ mol L}^{-1}$ in ethyl acetate.

Fig. 12 Two-photon absorption cross sections of compounds **5** (a) and **6** (b) in 680-900 and 680-960 nm regions, respectively.

Fig. 13 (a) One-photon fluorescence microscopy image of HepG2 cells stained with **1** with excitation at 405 nm. (b) Bright-field image. (c) Merged image.

Fig. 14 (a) One-photon fluorescence microscopy image of HepG2 cells stained with **5** with excitation at 405 nm. (b) Two-photon fluorescence microscopy image of HepG2 cells stained with **5** with excitation at 800 nm. (c) Bright-field image. (d) Merged image.

Scheme 1 Synthetic routes to target compounds **1–6**.

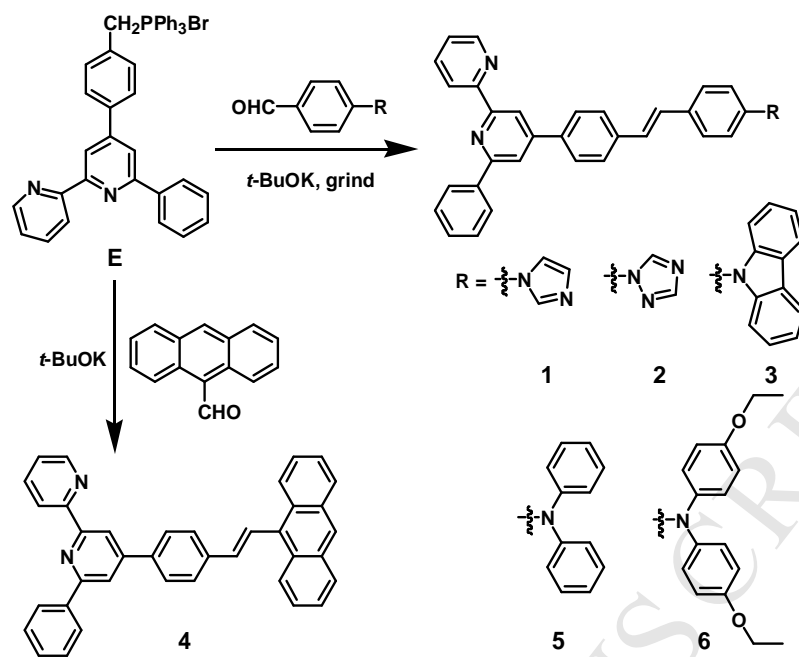
Table 1 The photophysical properties of compounds **1–6**.

ACCEPTED MANUSCRIPT

Table 1 The photophysical properties of dyes 1–6

	solvents	λ_{\max}^a	$\text{Log } \epsilon_{\max}^b$	λ_{\max}^c	$\Delta\nu^d$	Φ^e	λ_{\max}^f	σ^g	τ^h	τ^i
1	DCM	332	4.81	410	5730	0.78			0.86	0.75
	ethyl acetate	338	4.83	410	5430	0.81			0.89	0.76
	ethanol	335	4.84	417	5959	0.75			0.92	0.77
	acetonitrile	332	4.83	420	6041	0.70			1.03	0.79
	DMF	341	4.80	426	5851	0.73			1.10	0.83
2	DCM	337	4.82	406	5043	0.80			0.84	0.70
	ethyl acetate	335	4.88	404	5098	0.74			0.82	0.62
	ethanol	336	4.84	408	5252	0.70			0.87	0.70
	acetonitrile	334	4.83	410	5550	0.71			0.89	0.71
	DMF	341	4.80	416	5287	0.76			1.00	0.76
3	DCM	289, 339	4.54	450	7276	0.61			1.62	1.49
	ethyl acetate	289, 336	4.64	439	6983	0.65			1.38	1.28
	ethanol	288, 337	4.60	459	7887	0.59			1.82	1.45
	acetonitrile	288, 339	4.59	469	8177	0.56			2.17	1.62
	DMF	289, 341	4.50	468	7958	0.50			2.04	1.51
4	DCM	367, 386	4.14	492	5581	0.21			2.53	1.94
	ethyl acetate	366, 386	4.22	488	5414	0.25			2.68	2.18
	ethanol	367, 386	4.18	495	5704	0.20			2.58	1.93
	acetonitrile	367, 383	4.17	493	5825	0.13			2.22	1.30
	DMF	368, 389	3.99	498	5626	0.15			2.48	2.73
5	DCM	295, 387	4.63	505	6038	0.56	518	1378	2.06	1.75
	ethyl acetate	294, 380	4.66	487	5781	0.58	510	720	1.84	1.74
	ethanol	294, 382	4.61	518	6873	0.42	555	1012	1.80	1.70
	acetonitrile	295, 383	4.65	524	7026	0.41	557	1116	2.45	1.60
	DMF	295, 389	4.58	524	6623	0.45	557	1220	2.42	1.83
6	DCM	298, 398	4.68	551	6977	0.51	579	1654	2.67	1.66
	ethyl acetate	295, 394	4.70	525	6333	0.56	555	1547	2.97	1.73
	ethanol	295, 403	4.78							
	acetonitrile	294, 398	4.72							
	DMF	295, 404	4.66							

^a Absorption peak position in nm (1×10^{-5} mol L⁻¹). ^b Maximum molar absorbance. ^c Peak position of SPEF in nm, excited at the absorption maximum. ^d Stokes shift in cm⁻¹. ^e Quantum yields determined by using an integrating sphere. ^f TPEF peak position in nm pumped by femtosecond laser pulses at 300 mw at their maximum excitation wavelength. ^g 2PA cross section in GM. ^h The fitted fluorescence lifetime in ns. ⁱ The calculated fluorescence lifetime.



Scheme 1

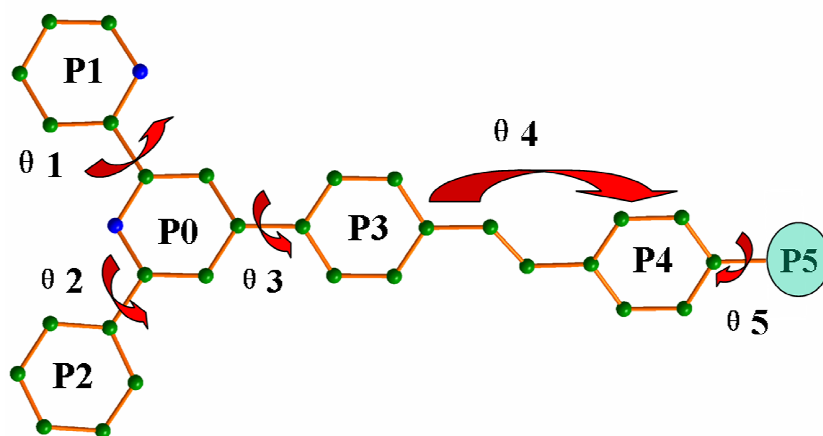


Fig. 1

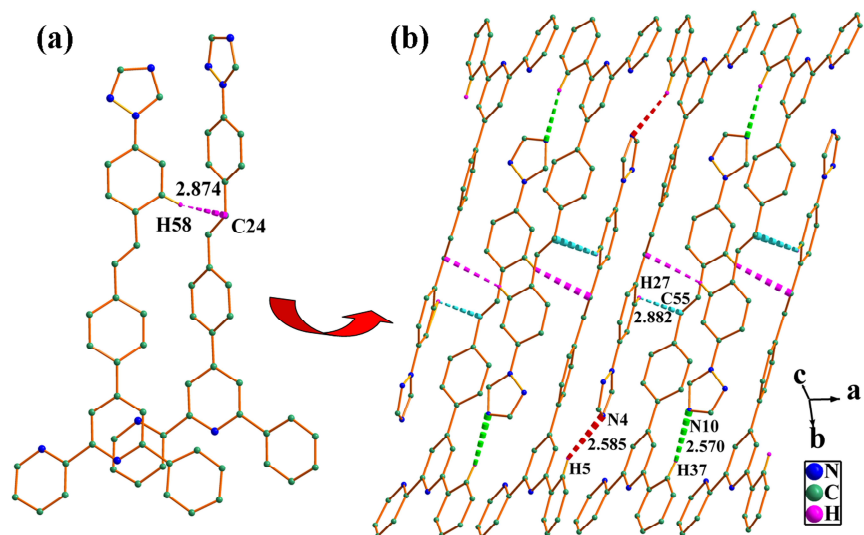


Fig. 2

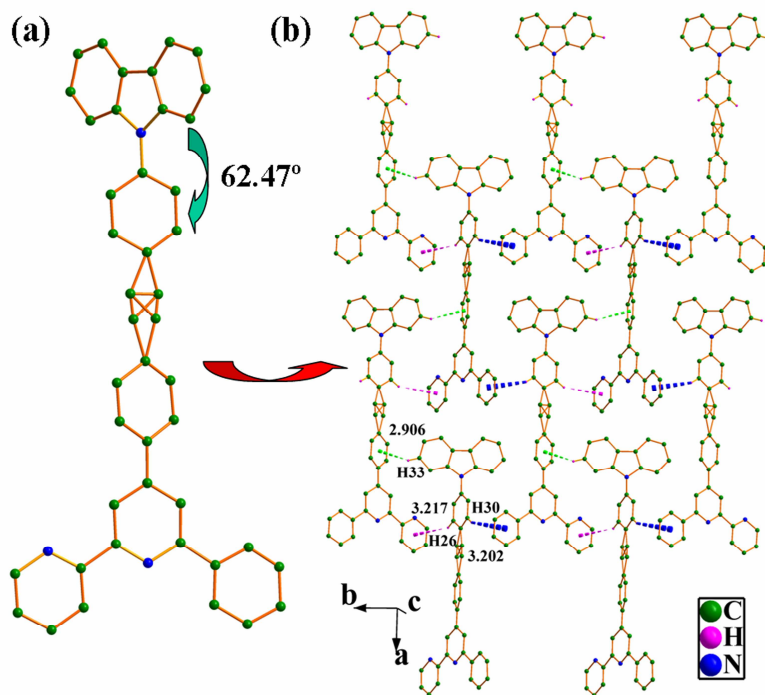


Fig. 3

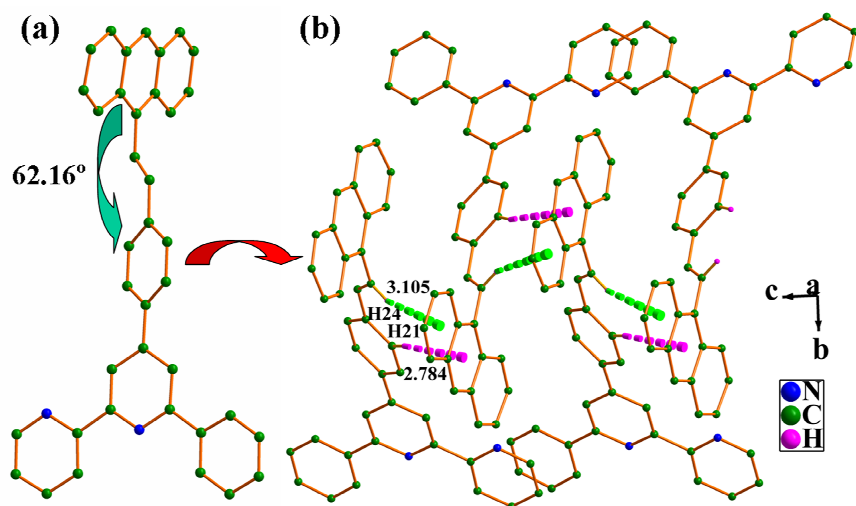


Fig. 4

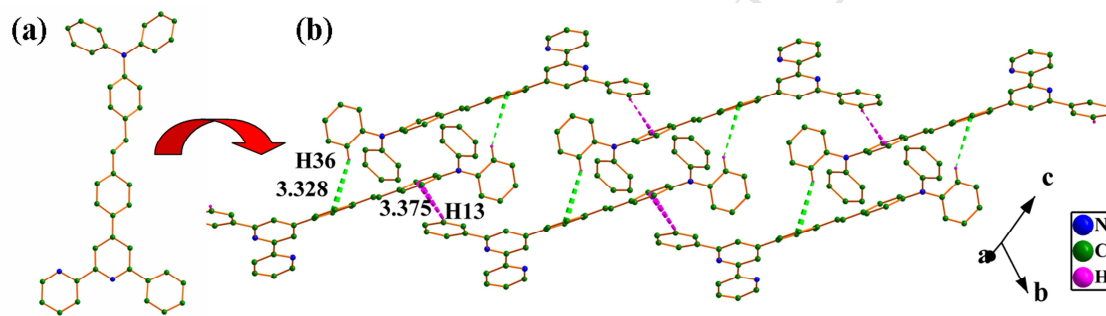


Fig. 5

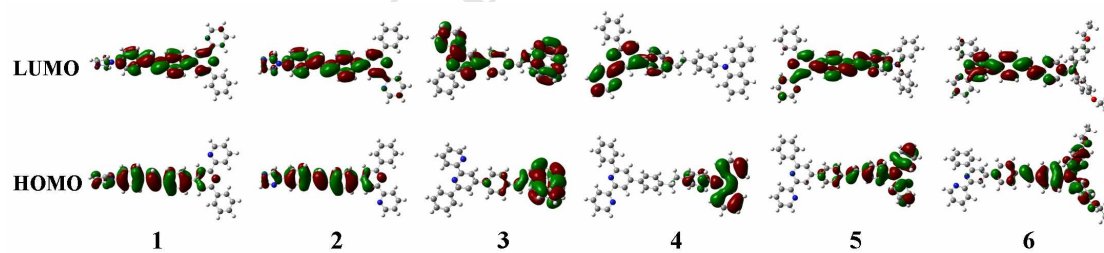


Fig. 6

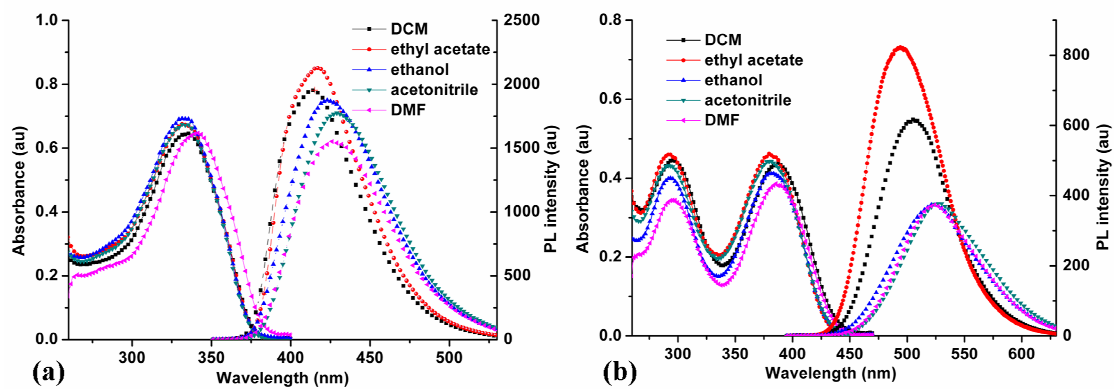


Fig. 7

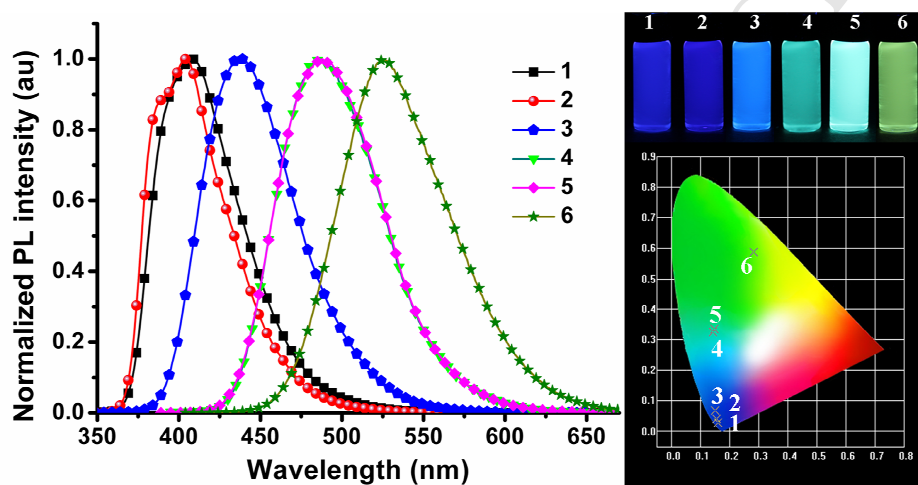


Fig. 8

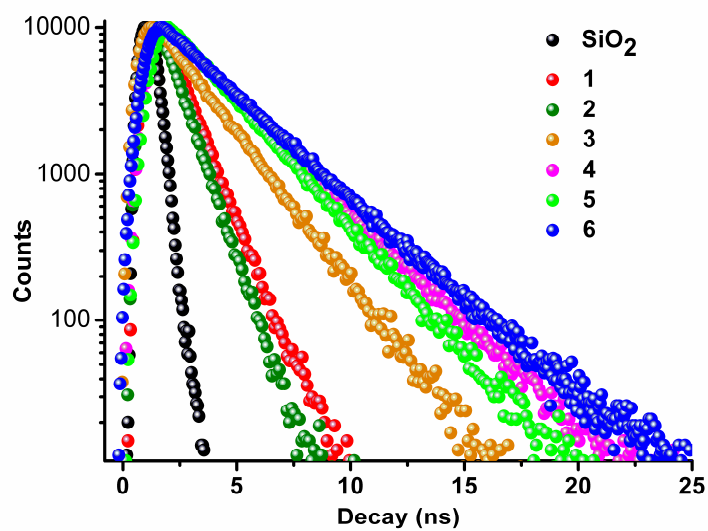


Fig. 9

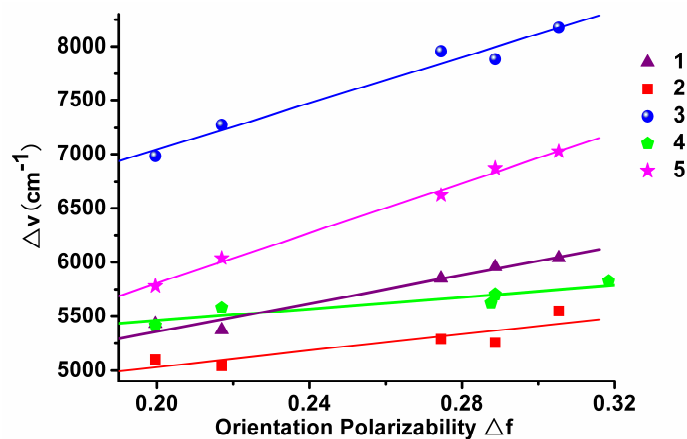


Fig. 10

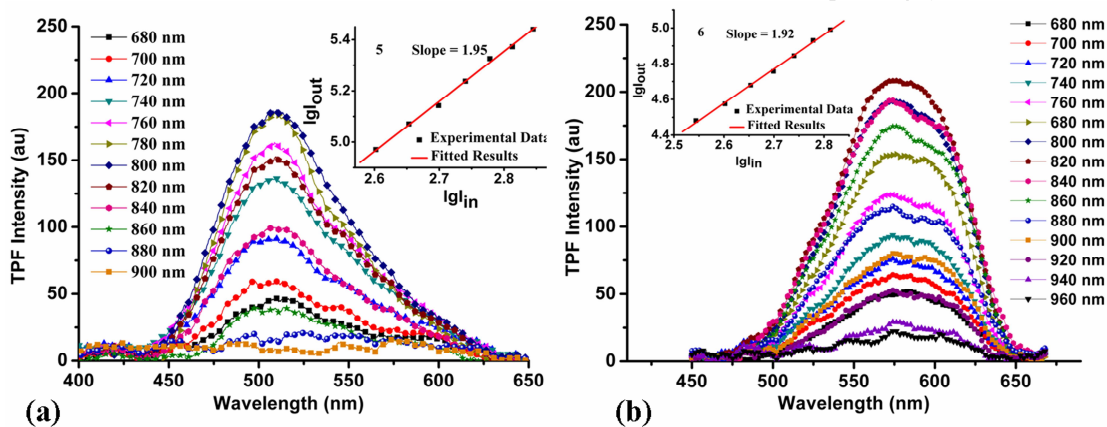


Fig. 11

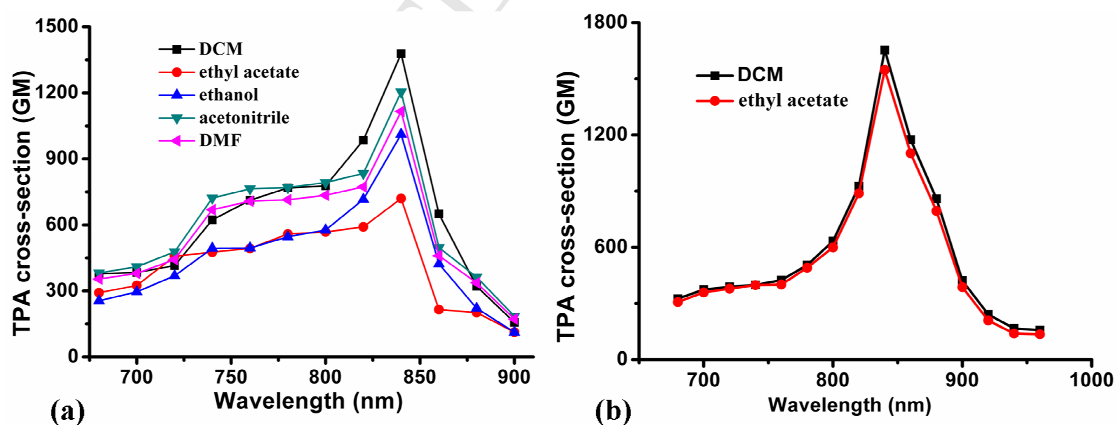


Fig. 12

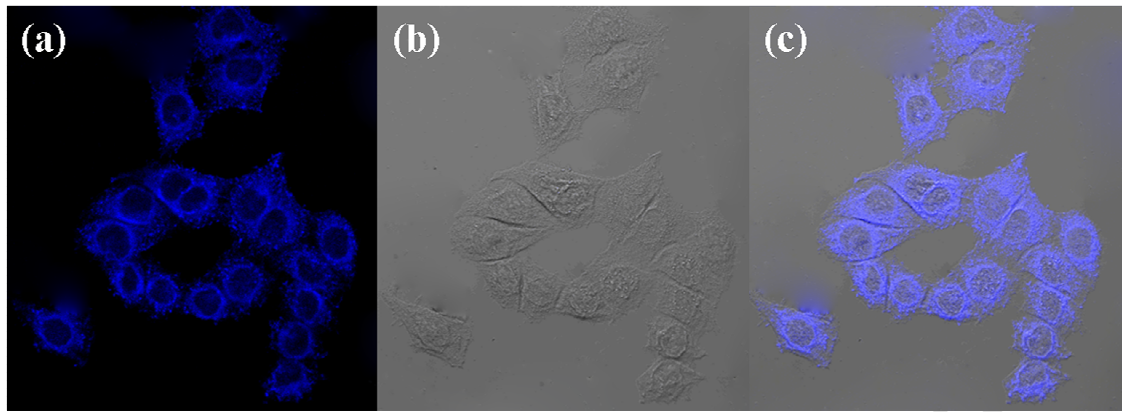


Fig. 13

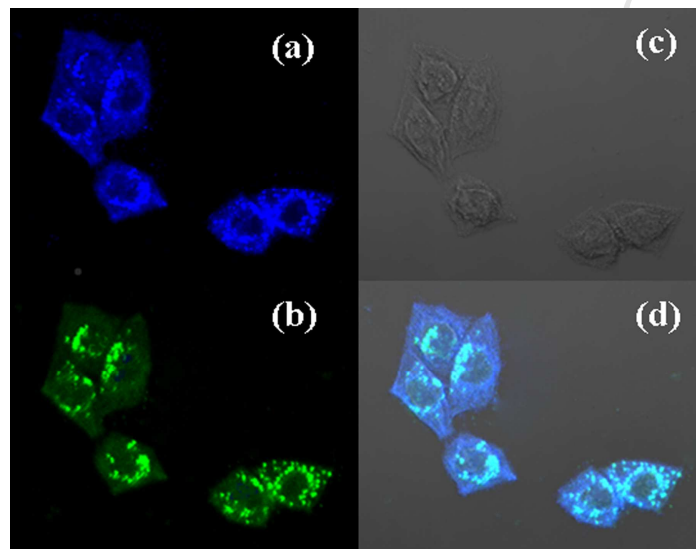


Fig. 14

1. Six new dyes with various electron donors were synthesized in high yield through simple reactions.
2. The optical properties of the dyes were successfully tuned by the different electron donors.
3. All dyes in solution show strong one-photon excited fluorescence and high quantum yield.
4. Dyes **5** and **6** exhibit strong TPEF with large TPA cross-section.
5. OPFM and TPFM imaging of them in HepG2 cell line was demonstrated.

Supporting Information for

New conjugated organic dyes with various electron donors: one- and two-photon excited fluorescence, and bioimaging

Feng Jin^{a, b}, Dong-Ling Xu^a, Hui-Zhi Zhu^a, Yan Yan^a, Jun Zheng^c, Jun Zhang^a,
Hong-Ping Zhou,^a * Jie-Ying Wu^a, Yu-Peng Tian^a

^aCollege of Chemistry and Chemical Engineering, Anhui University, Hefei 230039, P. R. China

^bDepartment of Chemistry, Fuyang Normal College, Fuyang 236041, P. R. China

^cCenter of Modern Experimental Technology, Anhui University, Hefei 230039, P. R. China

*Corresponding author. E-mail: zhpzhp@263.net (H. -P. Zhou).

Contents:

Syntheses of intermediates 1-3	Error! Bookmark not defined.
Figures S1-S3. MS of compounds 1-3	4
Figures S4-S6. MALDI-TOF-MS of compounds 4-6	5
Figures S7-S18. ¹ H NMR and ¹³ C NMR spectra of compounds 1-6	7
Table S1. Crystal Data and Refinement of compounds 2-5	13
Table S2. The dihedral angles between the neighboring connected aromatic rings in structures of compounds 2	13
Figure S19. The molecular structures of compounds 2-5	14
Table S3. Selected Bond Lengths (Å) of compounds 2-5	14
Figure S20. Linear absorption and emission spectra of compounds 2 (left) and 3 (right) in five organic solvents with a concentration of 1×10 ⁻⁵ mol/L	15
Figure S21. Linear absorption and emission spectra of compounds 4 (left) and 6 (right) in five organic solvents with a concentration of 1×10 ⁻⁵ mol/L	15
Figure S22. Time-resolved fluorescence curves of compounds 1 (left) and 2 (right) in five organic solvents	15
Figure S23. Time-resolved fluorescence curves of compounds 3 (left) and 4 (right) in five organic solvents	Error! Bookmark not defined.
Figure S24. Time-resolved fluorescence curves of compounds 5 (left) and 6 (right) in different organic solvents	Error! Bookmark not defined.
Figure S25. The TPEF spectra of 5 in DCM (left) and ethanol (right) pumped by femtosecond laser pulses at 300 mW under the different excitation wavelengths	Error! Bookmark not defined.
Figure S26. The TPEF spectra of 5 in acetonitrile (left) and DMF (right) pumped by femtosecond laser pulses at 300 mW under the different excitation wavelengths	Error! Bookmark not defined.

not defined.

FigureS27. The TPEF spectra of **6** in DCM pumped by femtosecond laser pulses at 300 mW under the different excitation wavelengths **Error! Bookmark not defined.**

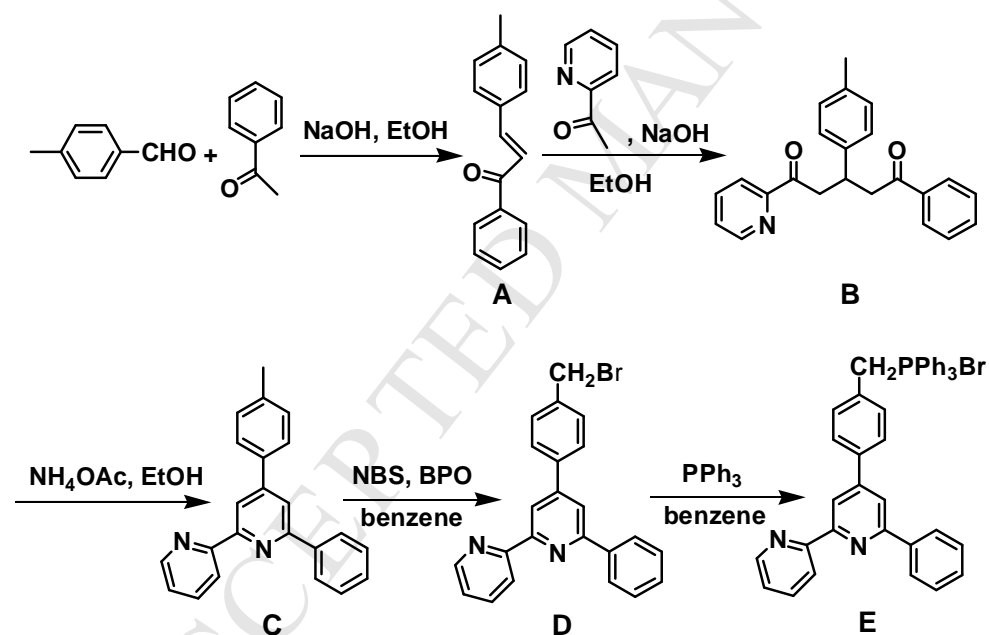
Figure S28. (a) The TPEF spectra of **3** in ethyl acetate pumped by femtosecond laser pulses at 300 mW under the different excitation wavelengths. (b) Output fluorescence (I_{out}) vs. the square of input laser power (I_{in}) for **3** **Error! Bookmark not defined.**

Figure S29. The TPEF spectra of compounds **5** (a) and **6** (b) pumped by femtosecond laser pulses at 300 mW under the optimal excitation wavelength at 800 nm for **5** and 820 nm for **6**.....**Error! Bookmark not defined.**

Figure S30. MTT assay of HepG2 cells treated with **1-6** at different concentrations for 24 h**Error! Bookmark not defined.**

Figures S31-34. Fluorescence microscopy image of HepG2 cells stained with compounds **2, 3, 4** and **6**..... **Error! Bookmark not defined.**

Syntheses of intermediates



Scheme S1. Synthetic routes to intermediates **A-E**.

Intermediate A. An aqueous NaOH solution (5%, 100 mL), p-methyl benzaldehyde (1.20 g, 10 mmol) and acetophenone (1.20 g, 10 mmol) were added in a round-bottom flask. The stirred mixture was refluxed at 85 °C for 8 h, and then cooled to room temperature. The precipitation was filtered and recrystallization with ethanol to afford the product as pale-yellow solid. Yield: 95%. Anal. Calcd. (%) for $C_{16}H_{14}O$: C, 86.45; H, 6.35. Found (%): C, 86.79; H, 6.81. FT-IR (KBr, cm^{-1}): 3049, 1655, 1597, 1334,

982, 690. ^1H NMR (CDCl_3 , 400 MHz): δ 2.39 (s, 3H), 7.23 (d, $J = 8.00$ Hz, 2H), 7.80 (d, $J = 15.7$ Hz, 1H), 7.53 (m, 6H), 8.02(m, 2H).

Intermediates B and C. Compound **A** (6.66 g, 30 mmol), acetylpyridine (3.63 g, 30 mmol) and NaOH (3.6 g, 90 mmol) were placed in a mortar. The mixture was continuously ground for 30 min. After completion of the reaction (monitored by Thin Layer Chromatography (TLC)), intermediate **B** was generated and used directly in the next step without purification. The mixture, ethanol (100 mL), and NH_4OAc (20.25 g, 450 mmol) was added to a round-bottom flask. The reaction mixture was kept stirring for 10 h at 85 °C. After cooled to room temperature, the precipitation was filtered, and it was purified by column chromatography on silica gel using petroleum ether/ethyl acetate (10/1, v/v) as the eluent to give the product as white solid **C**. Yield: 43%. Anal. Calcd. (%) for $\text{C}_{23}\text{H}_{28}\text{N}_2$: C, 85.68; H, 5.63; N, 8.69. Found (%): C, 86.11; H, 5.32; N, 8.97. FT-IR (KBr, cm^{-1}): 3055, 2922, 2849, 1584, 1385, 815, 789, 689. ^1H NMR (CDCl_3 , 400 MHz): δ 2.44 (s, 3H), 7.32 (t, 1H), 7.35 (t, 2H), 7.46(t, 1H), 7.51 (t, 2H), 7.74 (d, $J = 8.13$ Hz, 2H), 7.86 (m, 1H), 7.98 (d, $J = 1.11$ Hz, 1H), 8.64 (d, $J = 1.12$ Hz, 1H), 8.21(t, 2H), 8.68 (s, 1H), 8.72 (m, 1H). MS (ESI) (m/z): Calc. for $\text{C}_{23}\text{H}_{28}\text{N}_2$: 323.15 $[\text{M}]^+$; Found: 323.15 $[\text{M}]^+$.

Intermediates D and E. Compound **C** (3.22 g, 10 mmol), N-Bromosuccinimide (2.26 g, 12 mmol), and CCl_4 (100 mL) were added to a round-bottom flask. After stirring for 0.5 h at 80 °C, benzoyl peroxide (BPO, 0.1 g) was added. The reaction mixture was refluxed at 80 °C for 8 h. After cooled to room temperature, the precipitation was filtered and discarded. The filtrate containing intermediate **D** and triphenylphosphine (2.36 g, 9 mmol) were added to a round-bottom flask. The reaction mixture was refluxed at 80 °C for 12 h. The precipitation was collected by filtration and washed with isopropyl alcohol, and the intermediate **E** was obtained in 65% yield and used directly in the next step.

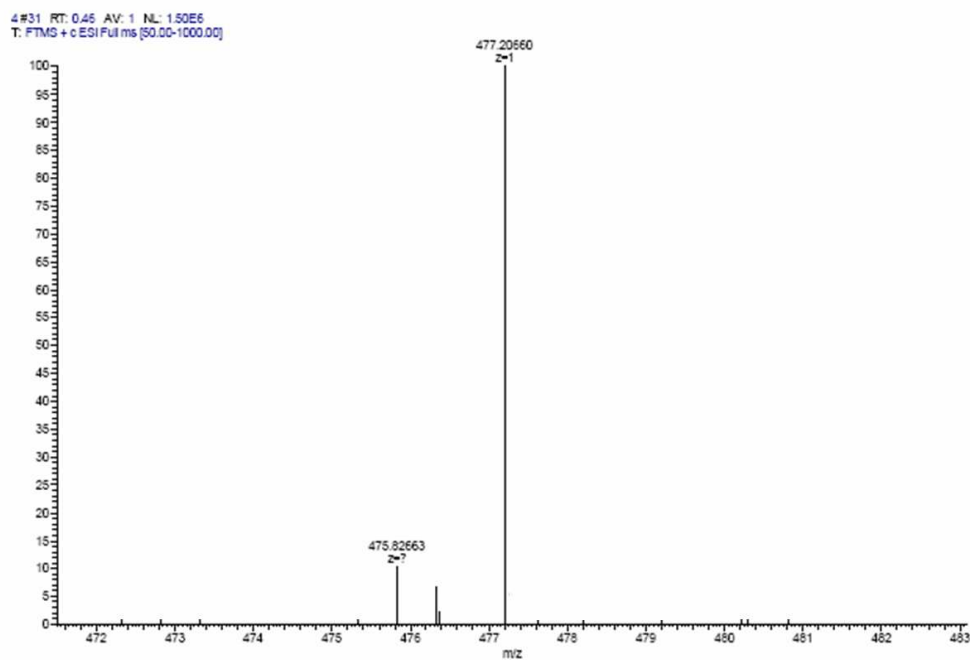


Fig. S1 MS of 1

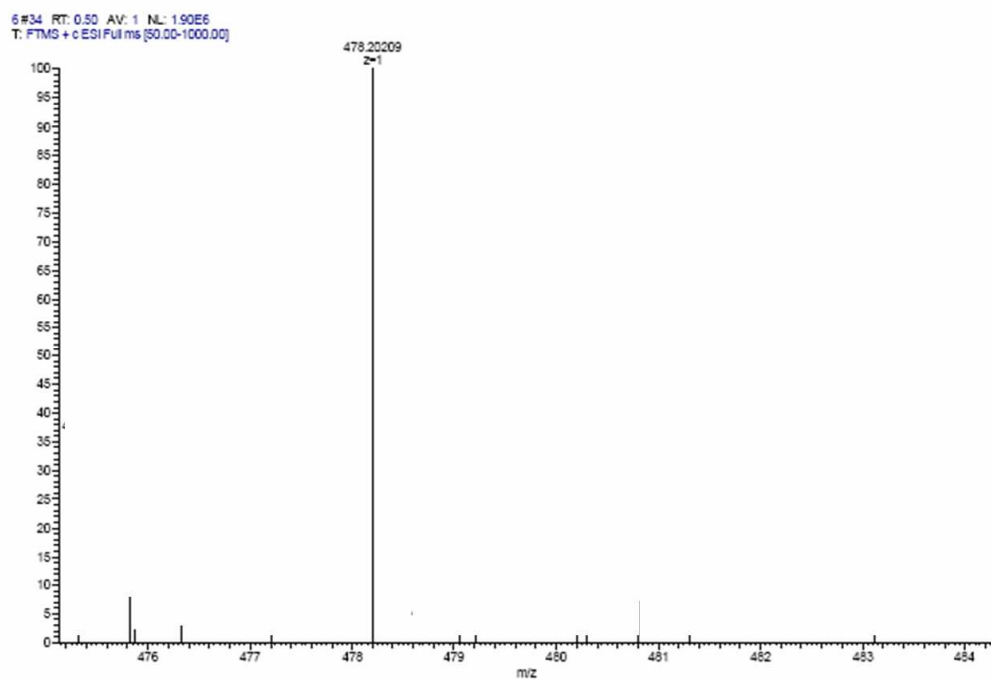


Fig. S2 MS of 2

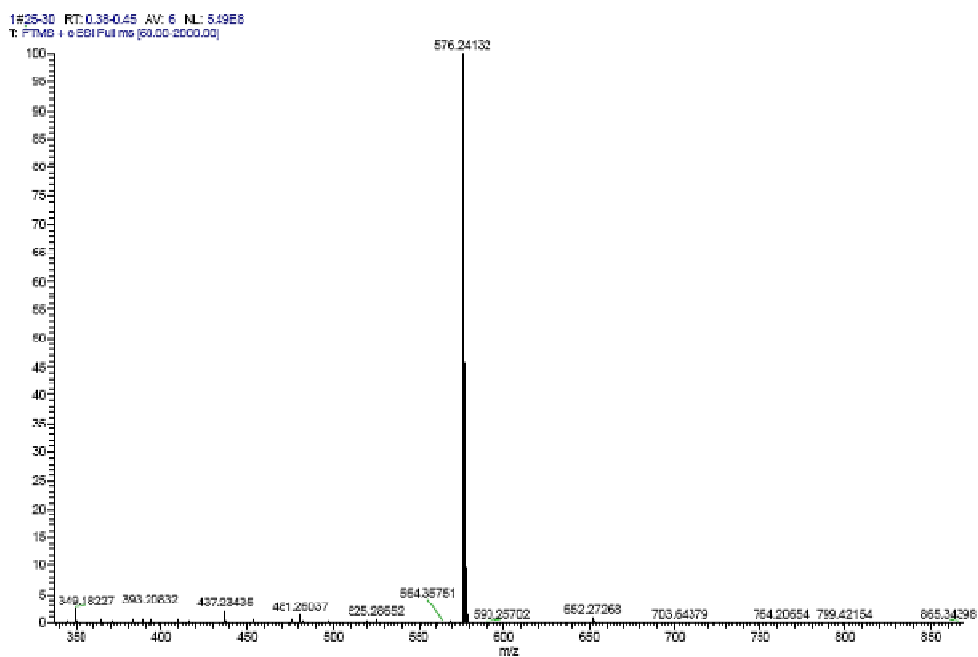


Fig. S3 MS of 3

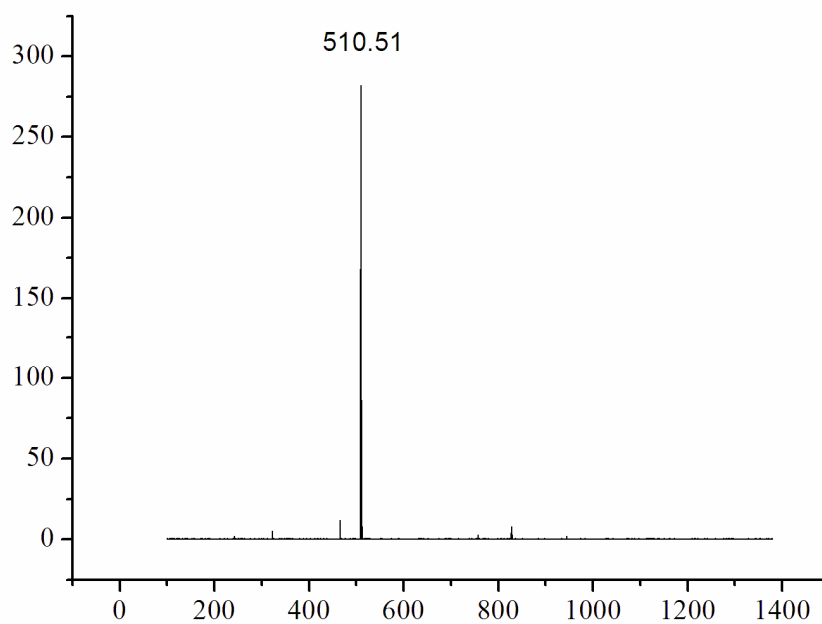
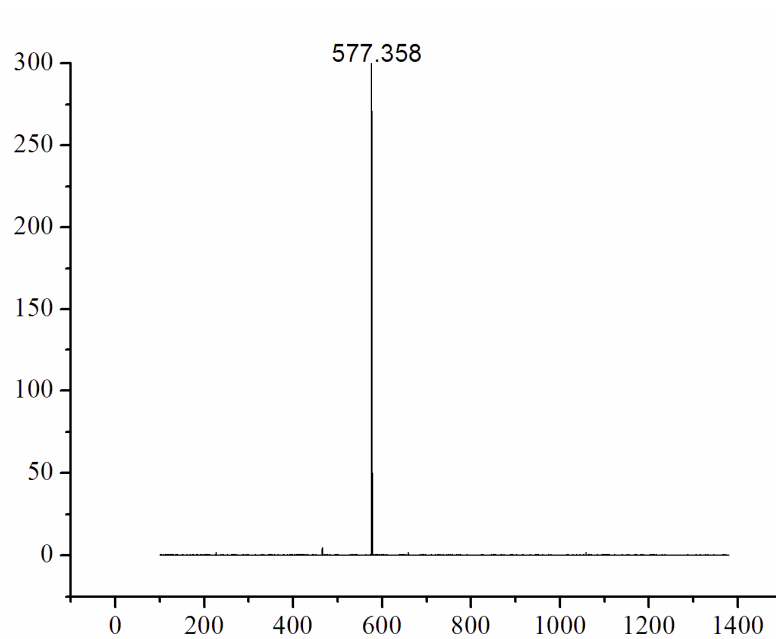
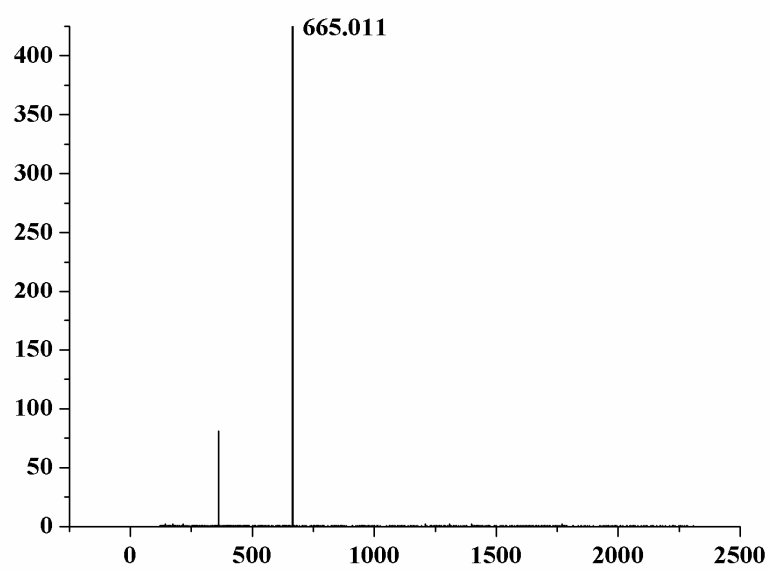
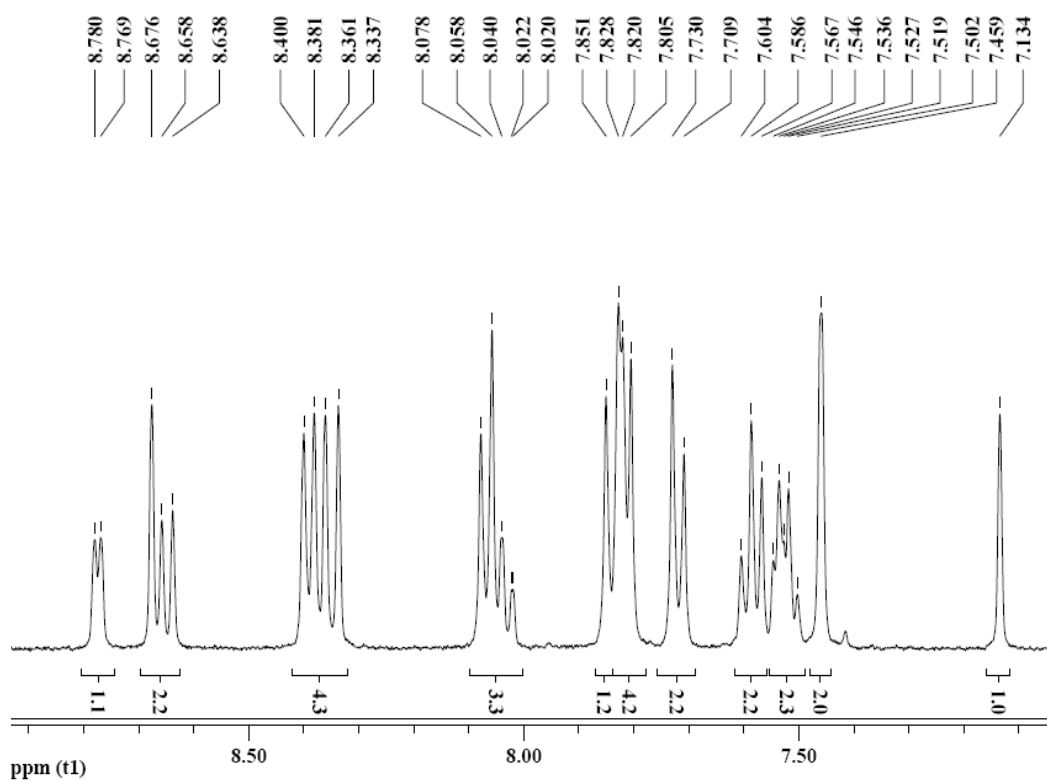
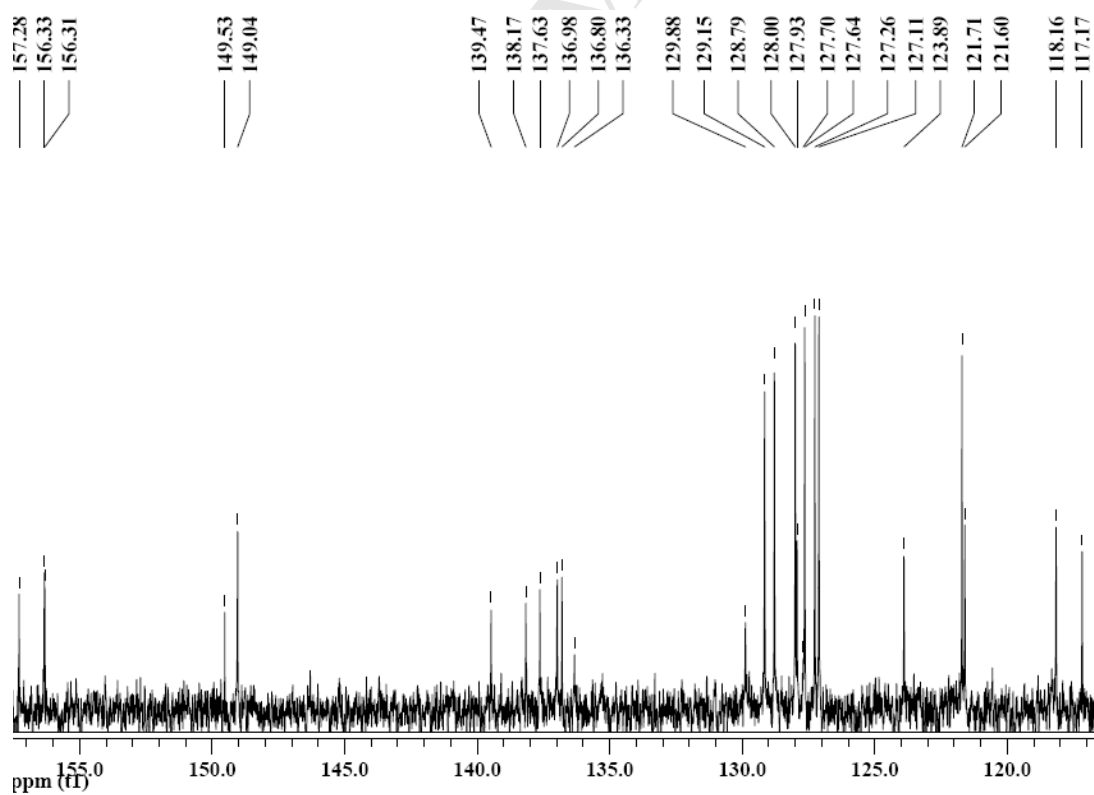
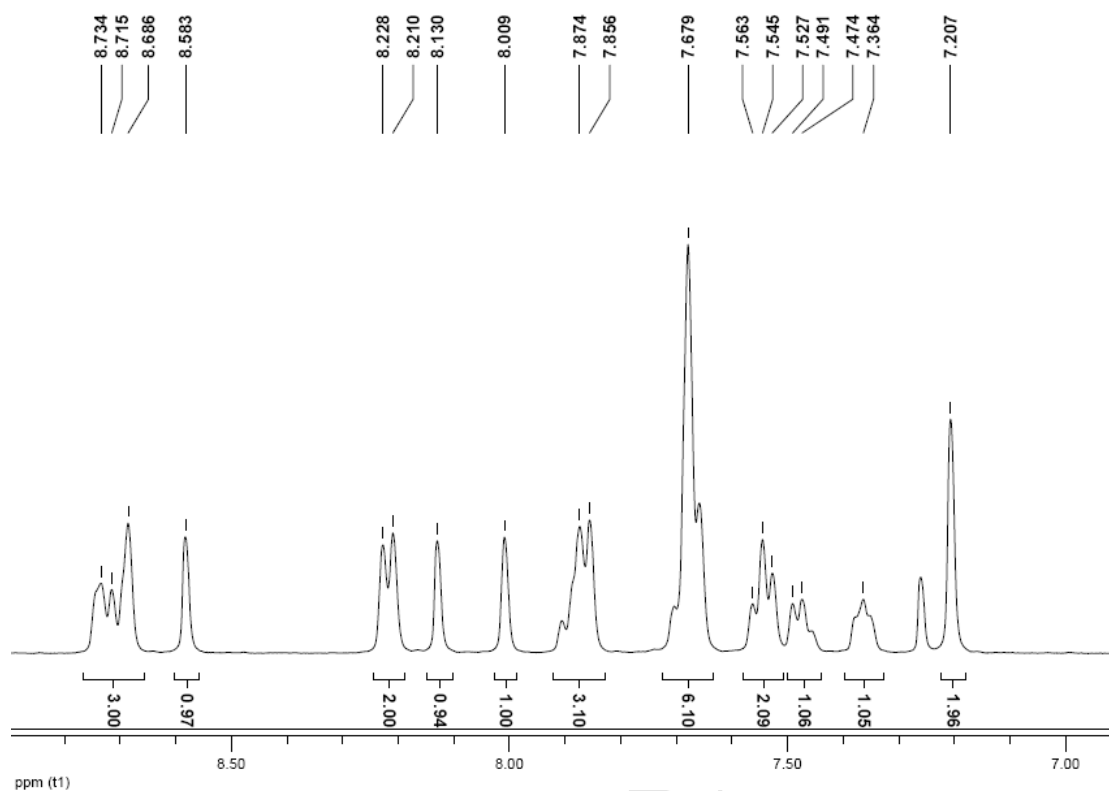
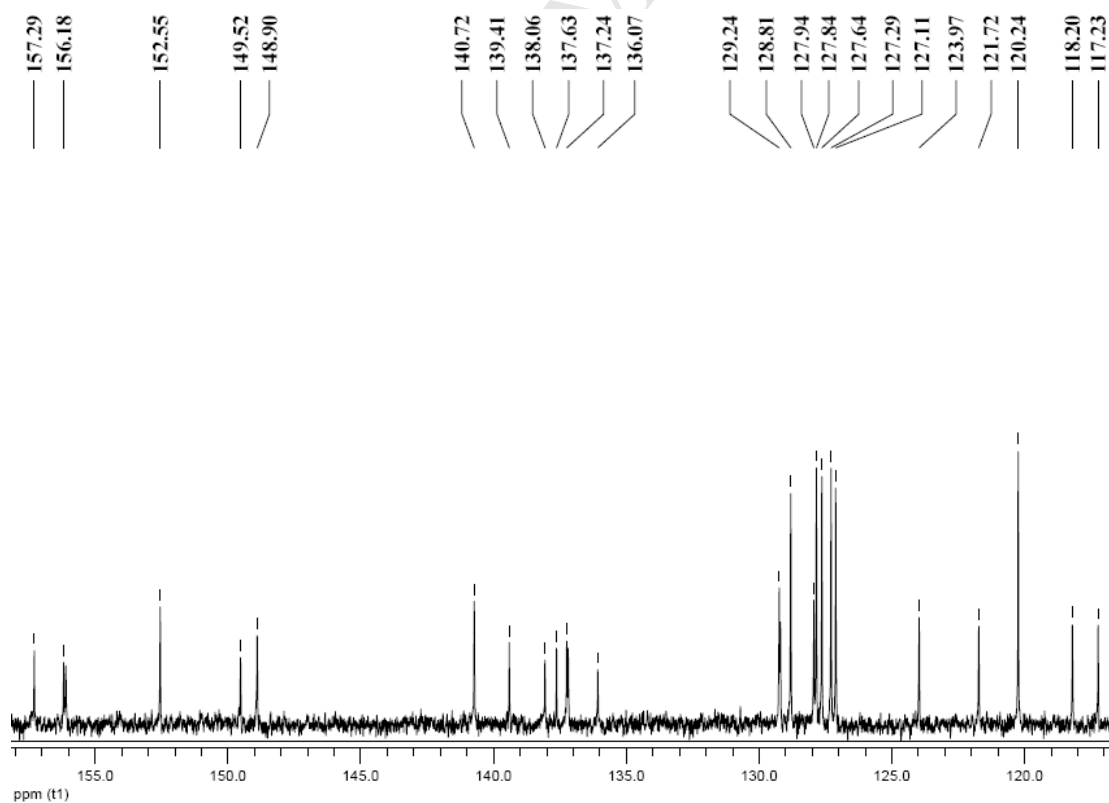
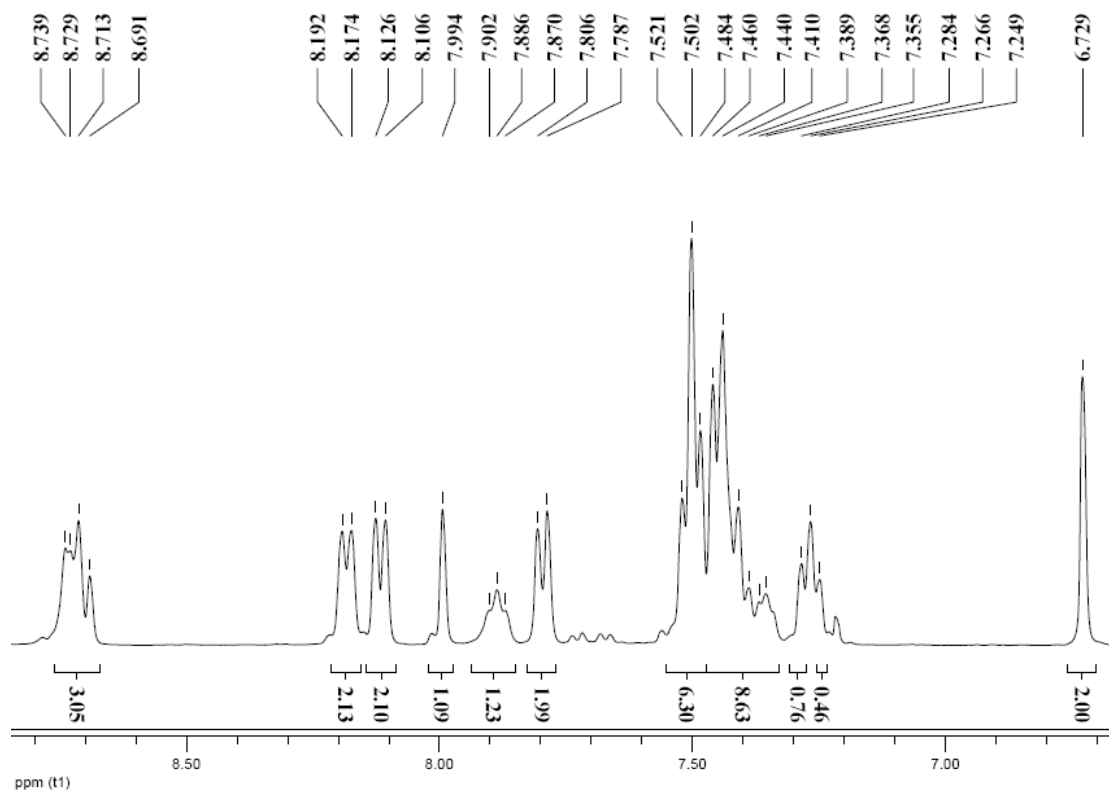
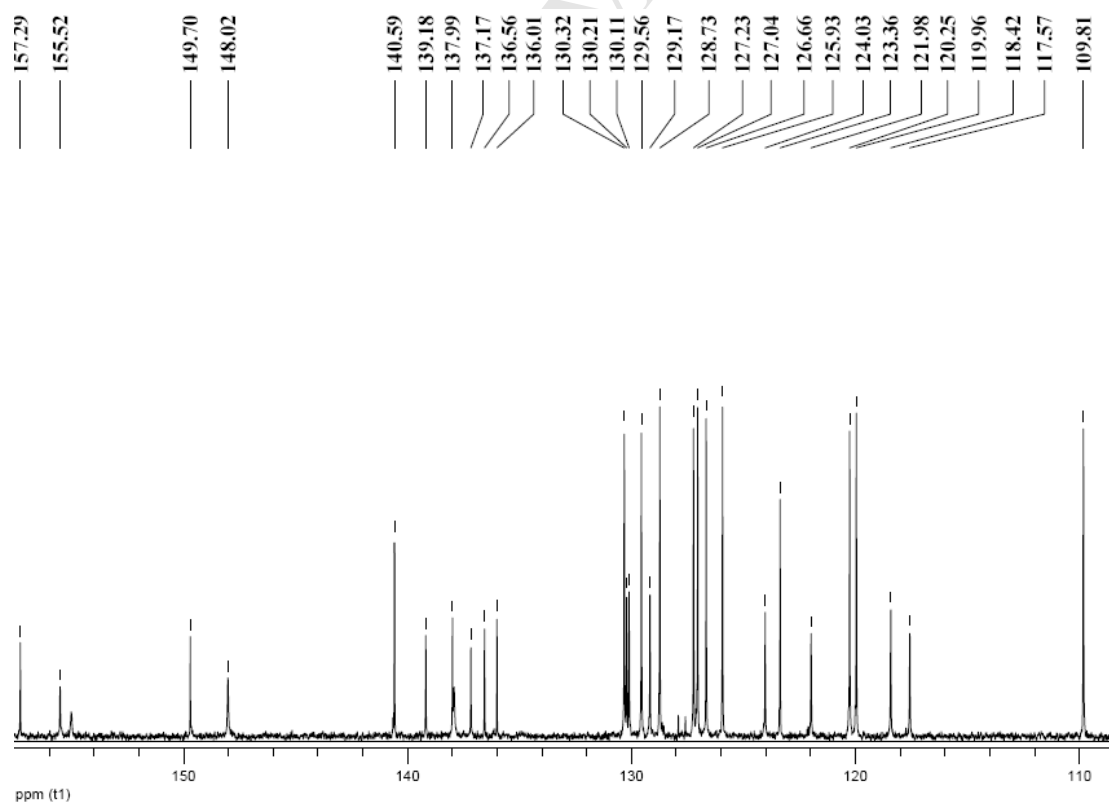


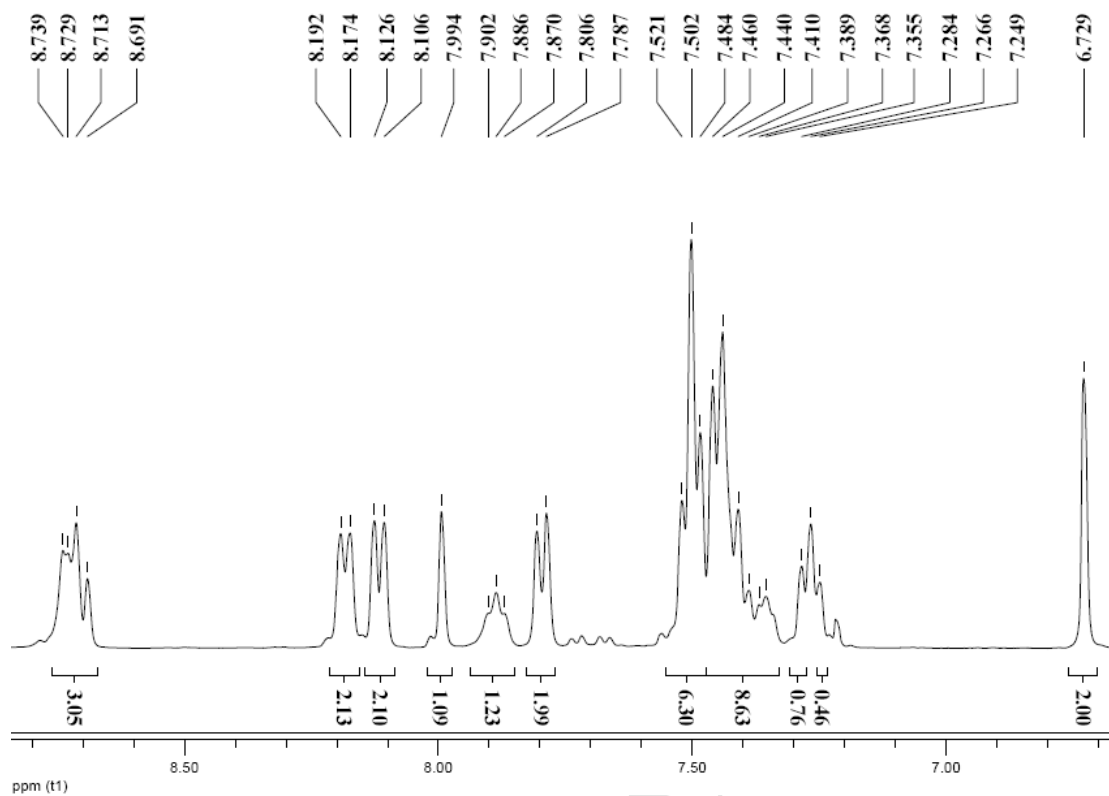
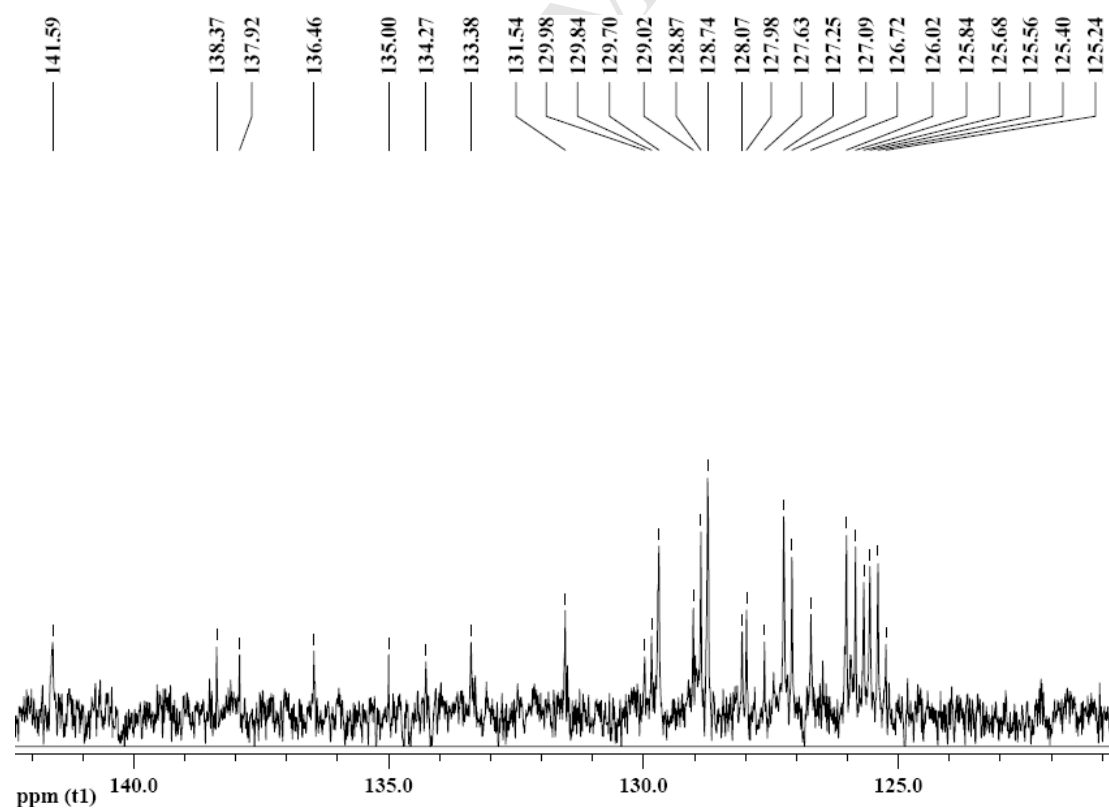
Fig. S4 MALDI-TOF MS of 4

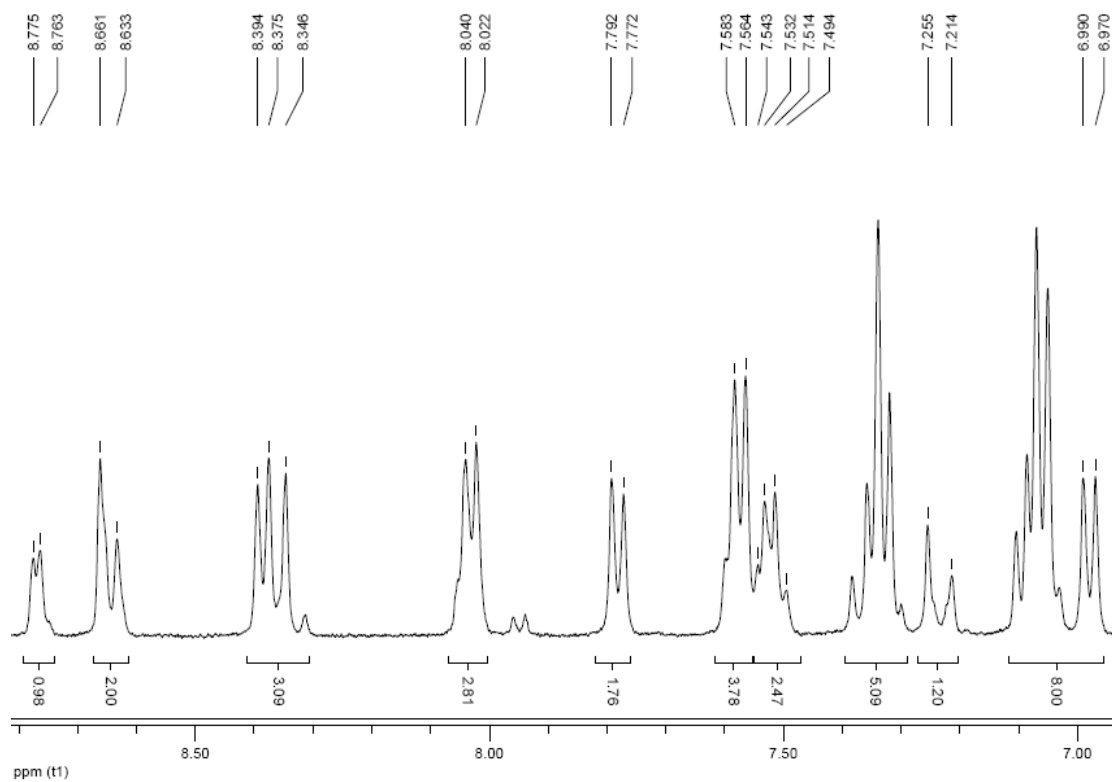
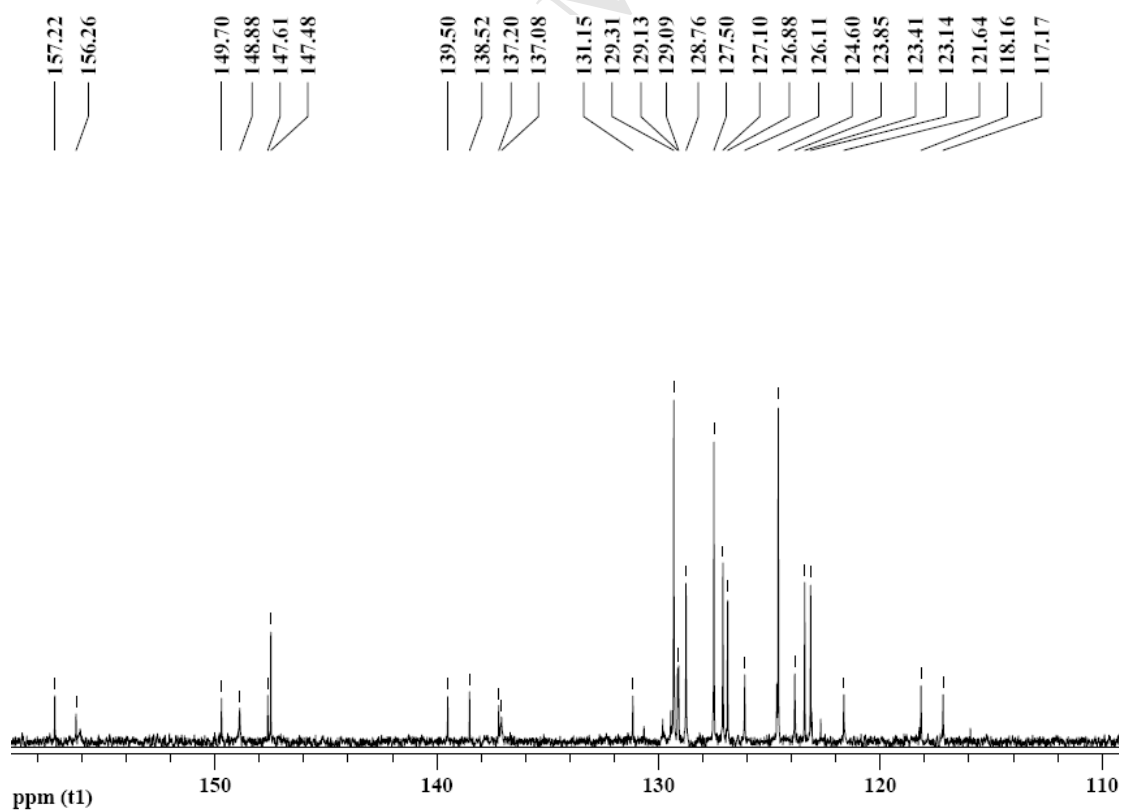
**Fig. S5** MALDI-TOF MS of **5****Fig. S6** MALDI-TOF MS of **6**

Fig. S7 ^1H NMR spectrum of **1**Fig. S8 ^{13}C NMR spectrum of **1**

Fig. S9 ^1H NMR spectrum of **2**Fig. S10 ^{13}C NMR spectrum of **2**

Fig. S11 ^1H NMR spectrum of **3**Fig. S12 ^{13}C NMR spectrum of **3**

Fig. S13 ^1H NMR spectrum of **4**Fig. S14 ^{13}C NMR spectrum of **4**

Fig. S15 ^1H NMR spectrum of **5**Fig. S16 ^{13}C NMR spectrum of **5**

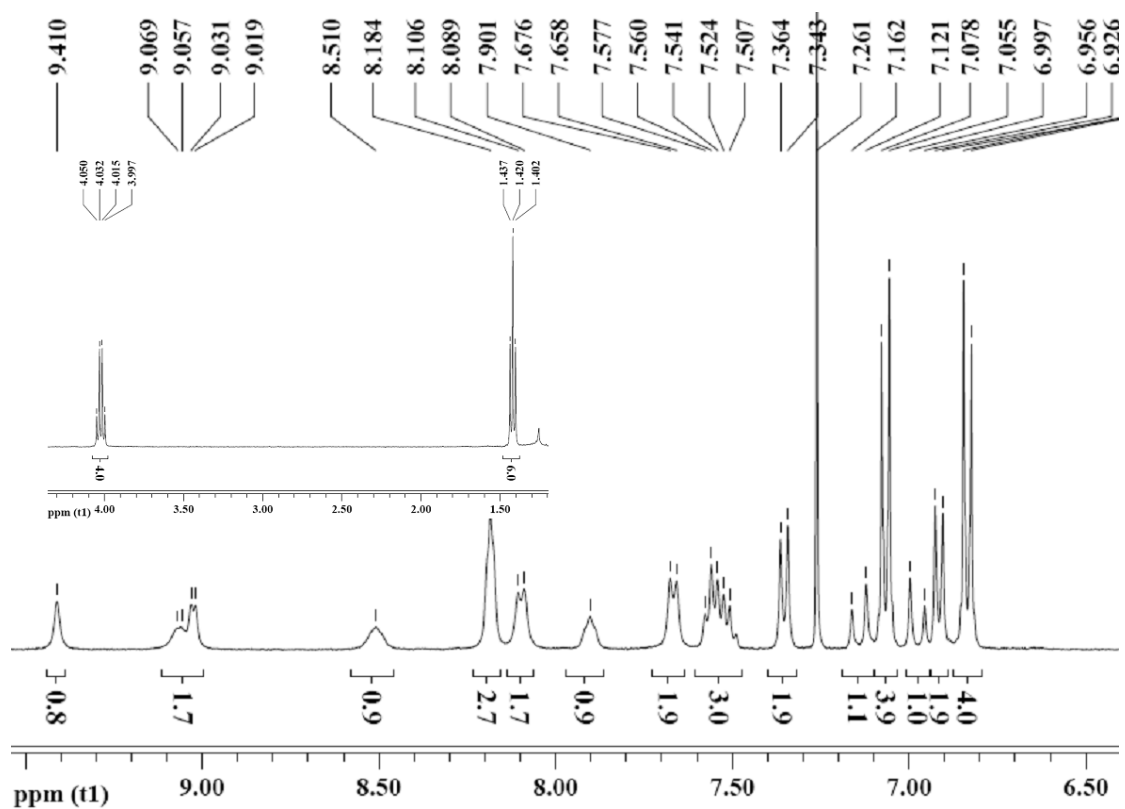
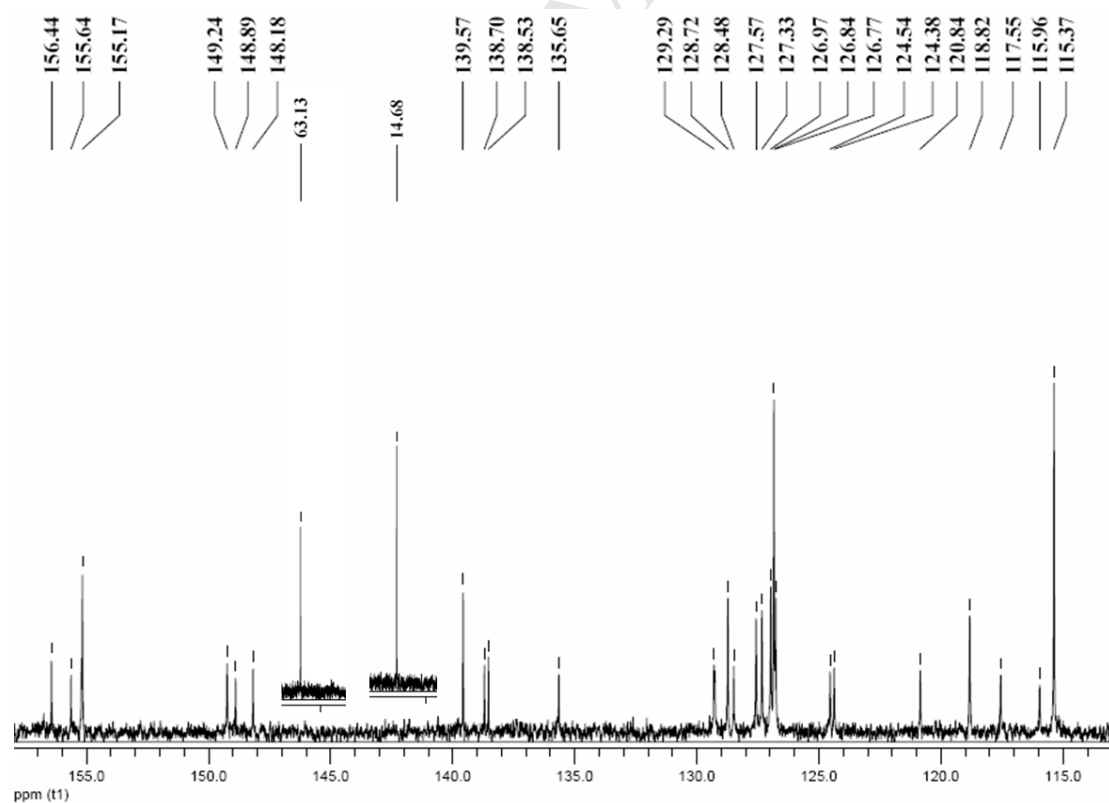
Fig. S17 ^1H NMR spectrum of **6**Fig. S18 ^{13}C NMR spectrum of **6**

Table S1 Crystal data and refinement of compounds **2-5**

Compound	2	3	4	5
empirical formula	C ₃₂ H ₂₃ N ₅	C ₃₈ H ₂₆ N ₂	C ₄₂ H ₂₉ N ₃	C ₄₂ H ₃₁ N ₃
formula weight	477.55	510.61	575.68	577.70
crystal system	Monoclinic,	Monoclinic	Orthorhombic	Triclinic
space group	<i>P</i> 2 ₁ / <i>c</i>	<i>P</i> 2 ₁ / <i>c</i>	<i>Pca</i> 2 ₁	<i>P</i> $\bar{1}$
<i>a</i> [Å]	9.574(5)	17.023(5)	23.11(4)	9.827(5)
<i>b</i> [Å]	48.010(5)	19.277(5)	13.64(2)	13.661(5)
<i>c</i> [Å]	11.378(5)	8.166(5)	9.88(2)	13.985(5)
α [°]	90.00	90.00	90.00	117.364(5)
β [°]	113.324(5)	90.696(5)	90.00	106.499(5)
γ [°]	90.00	90.00	90.00	91.151(5)
<i>V</i> [Å ³]	4802(3)	2680(2)	3116(9)	1574(1)
<i>Z</i>	8	4	4	2
<i>T</i> [K]	298(2)	298(2)	298(2)	298(2)
<i>D</i> calcd [g·cm ⁻³]	1.321	1.266	1.227	1.219
μ [mm ⁻¹]	0.080	0.074	0.072	0.071
θ range [°]	0.85-25.00	1.20-25.00	1.49-25.50	1.71-25.00
total no. data	34172	18951	7491	11236
no. unique data	8469	4710	4222	5490
no. params refined	668	361	426	406
<i>R</i> 1	0.0892	0.0494	0.0468	0.0506
<i>wR</i> 2	0.2269	0.1180	0.0788	0.1324
GOF on <i>F</i> ²	1.029	1.014	1.063	1.022

Table S2 The dihedral angles between the neighboring connected aromatic rings in structures of compounds **2-5**.

	01(P0-P1) (°)	02(P0-P2) (°)	03(P0-P3) (°)	04(P3-P4) (°)	05(P4-P5) (°)
Dye2	8.74/8.10	8.45/8.69	27.12/28.01	4.57/4.57	1.34/1.34
Dye3	1.55	2.35	24.59	18.36	62.47
Dye4	7.22	9.63	27.90	62.16	
Dye5	6.27	13.19	32.42	9.33	

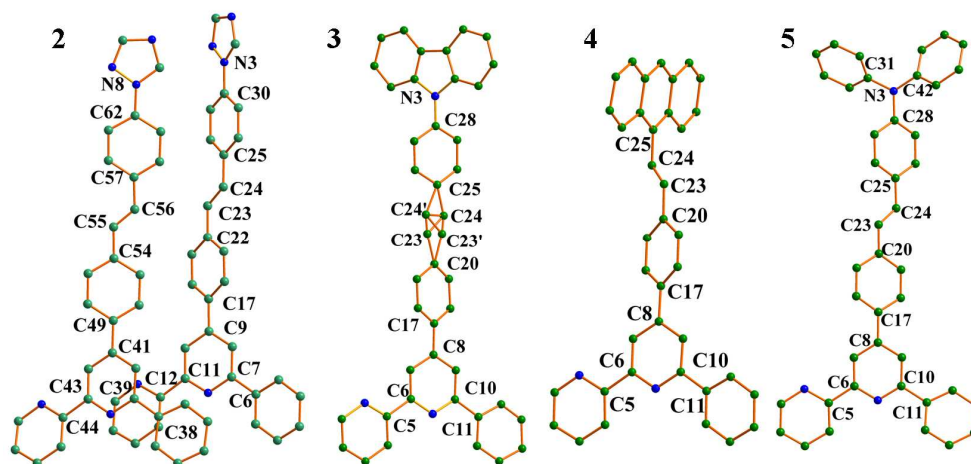


Fig. S19 The molecular structures of compounds **2-5**, together with the atom numbering scheme. Hydrogen atoms are omitted for clarity.

Table S3 Selected Bond Lengths (Å) and Angles (°) of compounds **2-5**

2					
C(7)–C(6)	1.482(7)	C(25)–C(24)	1.474(7)	C(55)–C(56)	1.264(7)
C(9)–C(17)	1.482(6)	N(3)–C(30)	1.428(6)	C(54)–C(55)	1.477(7)
C(22)–C(23)	1.459(6)	N(8)–C(62)	1.414(6)	C(41)–C(49)	1.477(6)
C(24)–C(23)	1.305(6)	C(57)–C(56)	1.474(7)	C(43)–C(44)	1.482(7)
C(39)–C(38)	1.489(7)				
3					
C(28)–N(3)	1.430(4)	C(24)–C(25)	1.53(1)	C(23)–C(24)	1.30(1)
C(20)–C(23)	1.53(1)	C(8)–C(17)	1.489(4)	C(5)–C(6)	1.53(1)
C(10)–C(11)	1.47(1)				
4					
C(5)–C(6)	1.486(4)	C(10)–C(11)	1.488(4)	C(17)–C(8)	1.490(3)
C(20)–C(23)	1.462(3)	C(25)–C(24)	1.484(3)	C(23)–C(24)	1.310(3)
5					
C(5)–C(6)	1.489(3)	C(11)–C(10)	1.487(3)	C(8)–C(17)	1.485(3)
C(20)–C(23)	1.462(3)	C(24)–C(23)	1.322(3)	C(24)–C(25)	1.465(3)
N(3)–C(42)	1.412(3)	N(3)–C(31)	1.421(3)	N(3)–C(28)	1.427(2)
C(31)–N(3)–C(28)	118.4(2)	C(31)–N(3)–C(42)	120.6(2)	C(42)–N(3)–C(28)	119.2(2)

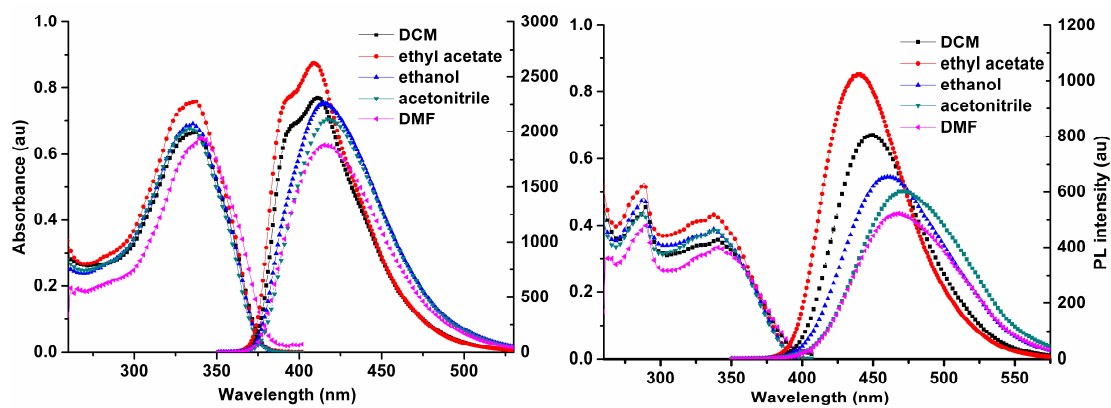


Fig. S20 Linear absorption and emission spectra of compounds **2** (left) and **3** (right) in five organic solvents with a concentration of 1×10^{-5} mol/L.

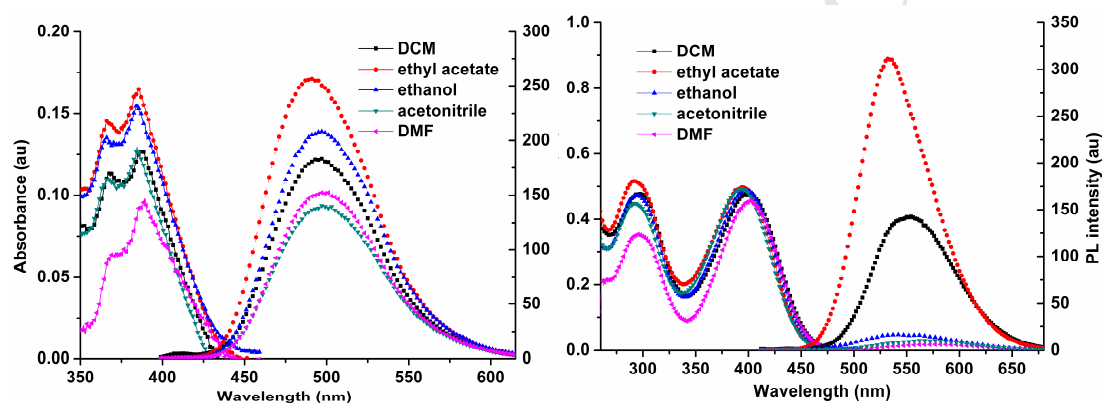


Fig. S21 Linear absorption and emission spectra of compounds **4** (left) and **6** (right) in five organic solvents with a concentration of 1×10^{-5} mol/L.

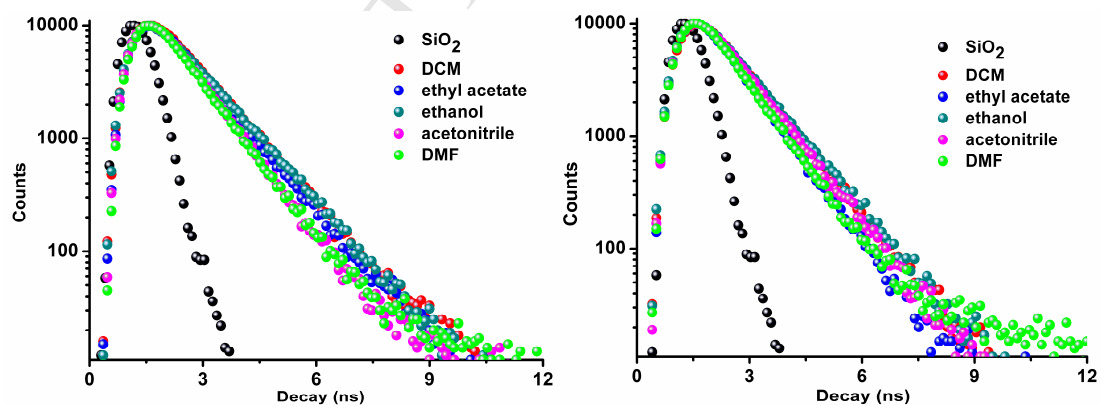


Fig. S22 Time-resolved fluorescence curves of compounds **1** (left) and **2** (right) in five organic solvents.

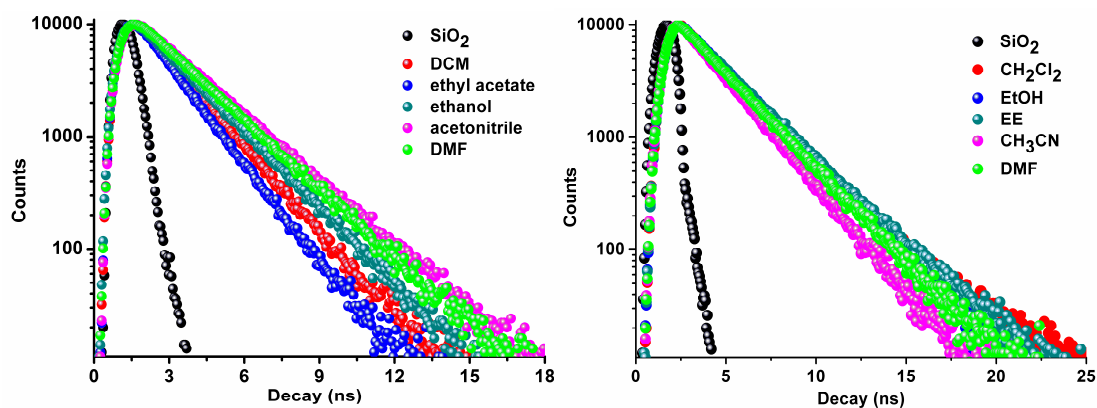


Fig. S23 Time-resolved fluorescence curves of compounds 3 (left) and 4 (right) in five organic solvents.

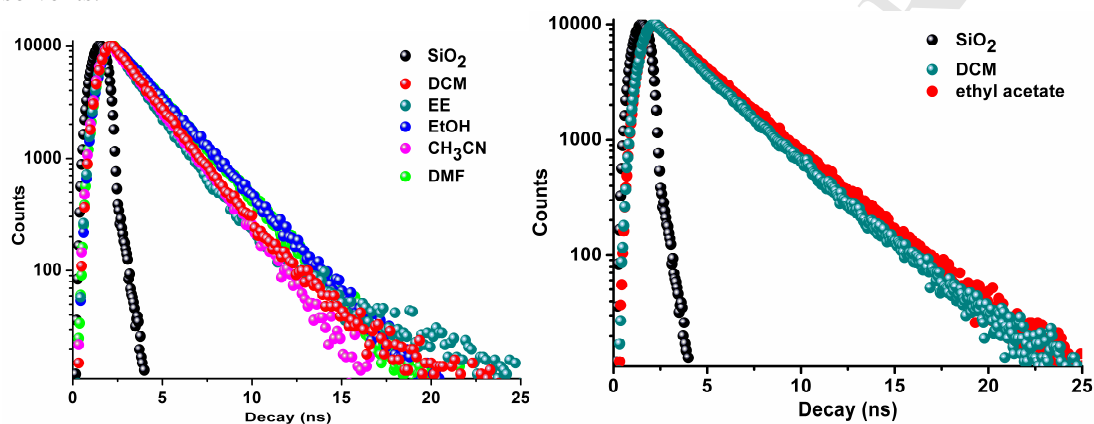


Fig. S24 Time-resolved fluorescence curves of compounds 5 (left) and 6 (right) in different organic solvents.

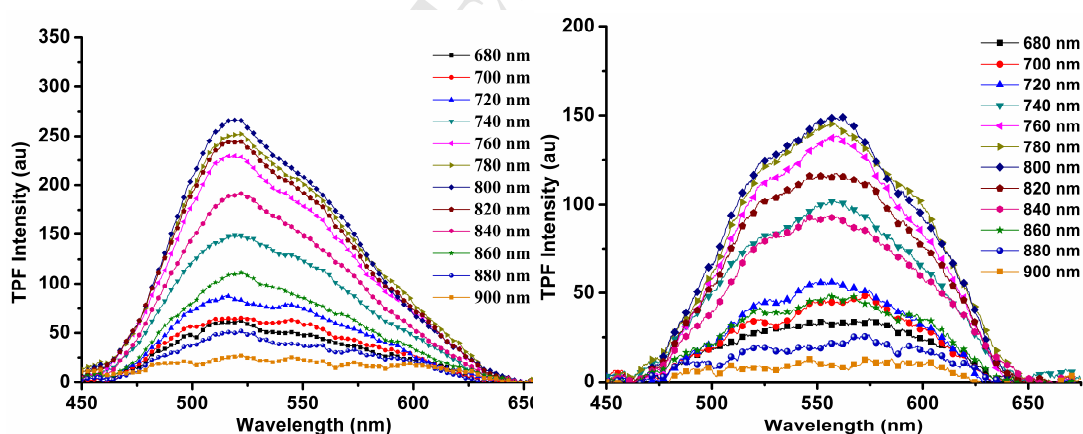


Fig. S25. The TPEF spectra of 5 in DCM (left) and ethanol (right) pumped by femtosecond laser pulses at 300 mW under the different excitation wavelengths.

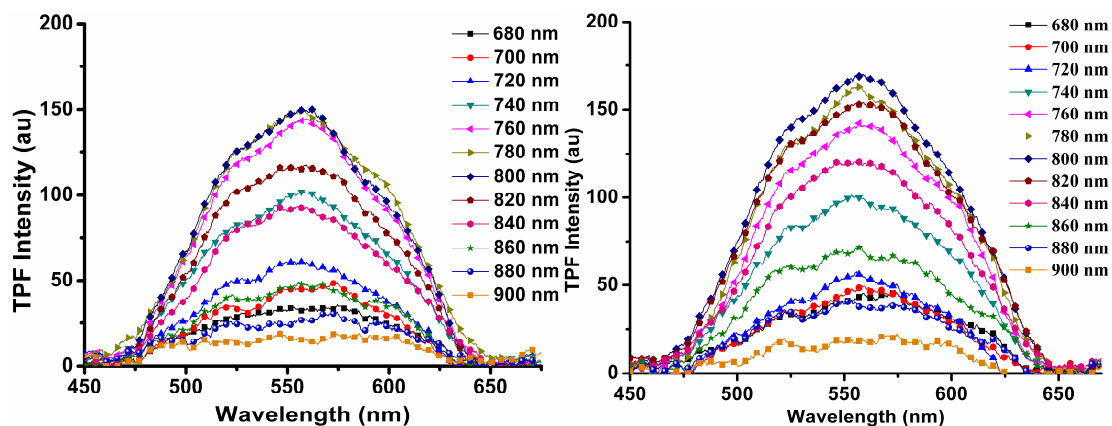


Fig. S26. The TPEF spectra of **5** in acetonitrile (left) and DMF (right) pumped by femtosecond laser pulses at 300 mW under the different excitation wavelengths.

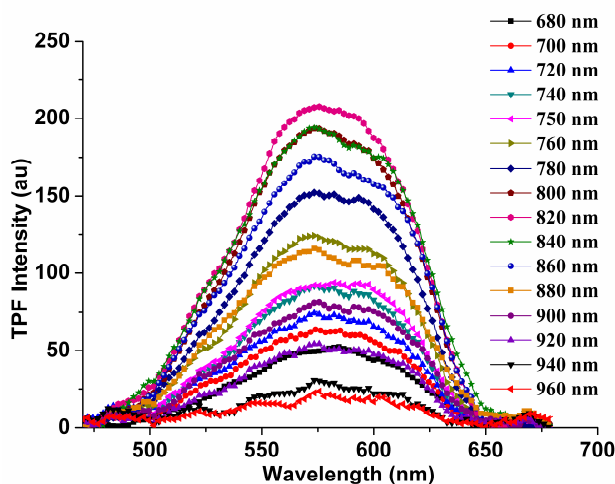


Fig. S27. The TPEF spectra of **6** in DCM pumped by femtosecond laser pulses at 300 mW under the different excitation wavelengths.

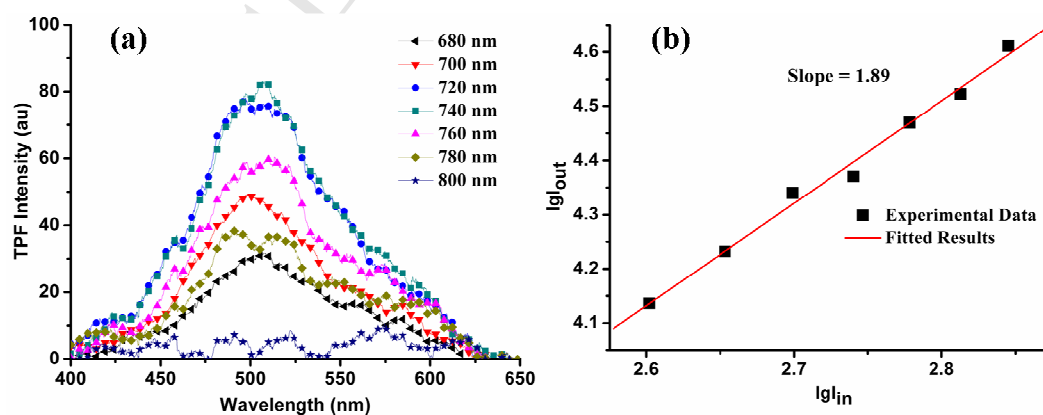


Fig. S28 (a) The TPEF spectra of **3** in ethyl acetate pumped by femtosecond laser pulses at 300 mW under the different excitation wavelengths. (b) Output fluorescence (I_{out}) vs. the square of input laser power (I_{in}) for **3**.

Supporting Information for

New conjugated organic dyes with various electron donors: one- and two-photon excited fluorescence, and bioimaging

Feng Jin^{a, b}, Dong-Ling Xu^a, Hui-Zhi Zhu^a, Yan Yan^a, Jun Zheng^c, Jun Zhang^a,
Hong-Ping Zhou,^{a, *} Jie-Ying Wu^a, Yu-Peng Tian^a

^aCollege of Chemistry and Chemical Engineering, Anhui University, Hefei 230039, P. R. China

^bDepartment of Chemistry, Fuyang Normal College, Fuyang 236041, P. R. China

^cCenter of Modern Experimental Technology, Anhui University, Hefei 230039, P. R. China

*Corresponding author. E-mail: zhpzhp@263.net (H. -P. Zhou).

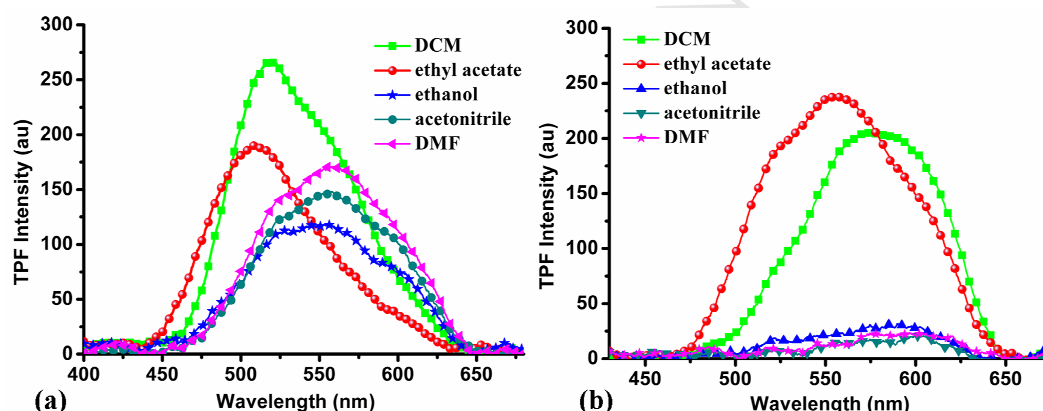


Fig. S29 The TPEF spectra of compounds **5** (a) and **6** (b) pumped by femtosecond laser pulses at 300 mW under the optimal excitation wavelength at 800 nm for **5** and 820 nm for **6**, with $c = 5.0 \times 10^{-4} \text{ mol L}^{-1}$ in different solvents.

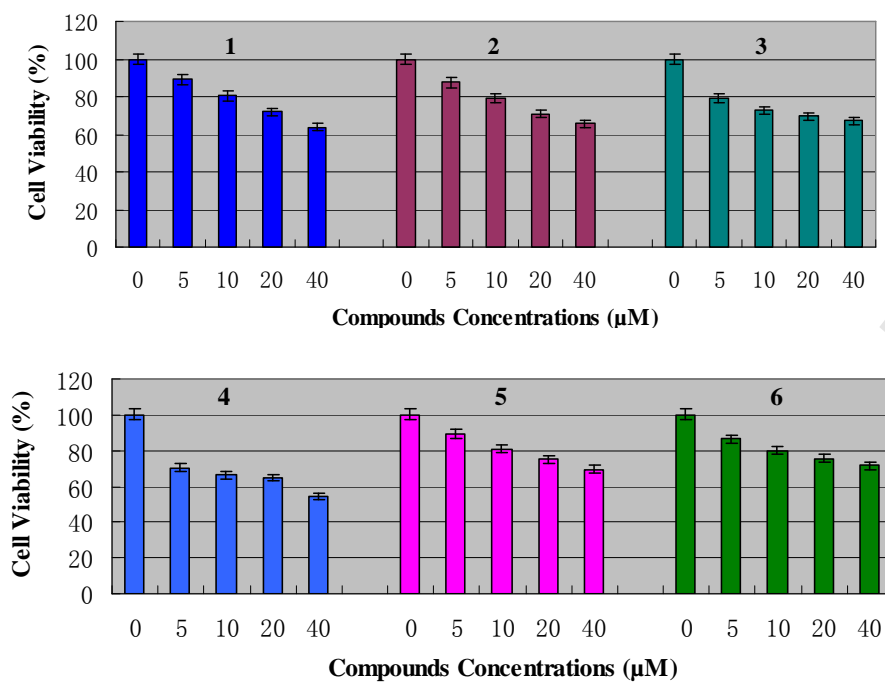


Fig. S30 MTT assay of HepG2 cells treated with 1-6 at different concentrations for 24 h.

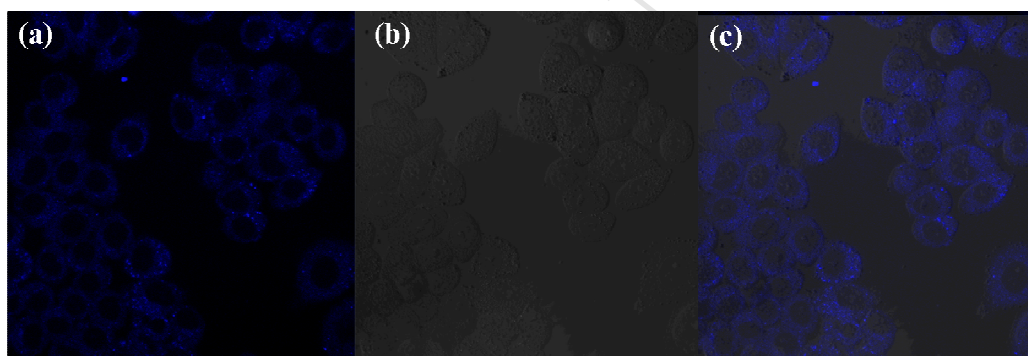


Fig. S31 (a) One-photon fluorescence microscopy image of HepG2 cells stained with 2 with excitation at 405 nm. (b) Bright-field image. (c) Merged image.

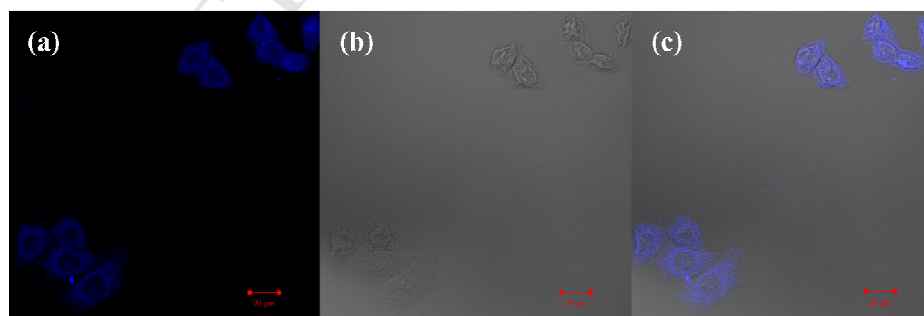


Fig. S32 (a) One-photon fluorescence microscopy image of HepG2 cells stained with 4 with excitation at 405 nm. (b) Bright-field image. (c) Merged image.

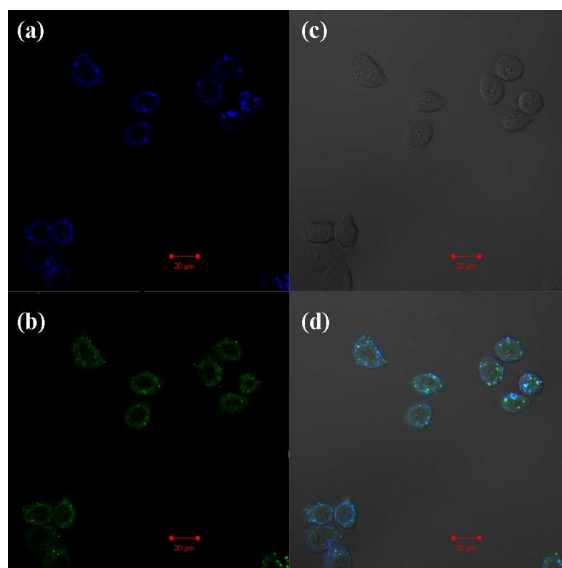


Fig. S33 (a) One-photon fluorescence microscopy image of HepG2 cells stained with **3** with excitation at 405 nm. (b) Two-photon fluorescence microscopy image of HepG2 cells stained with **3** with excitation at 800 nm. (c) Bright-field image. (d) Merged image.

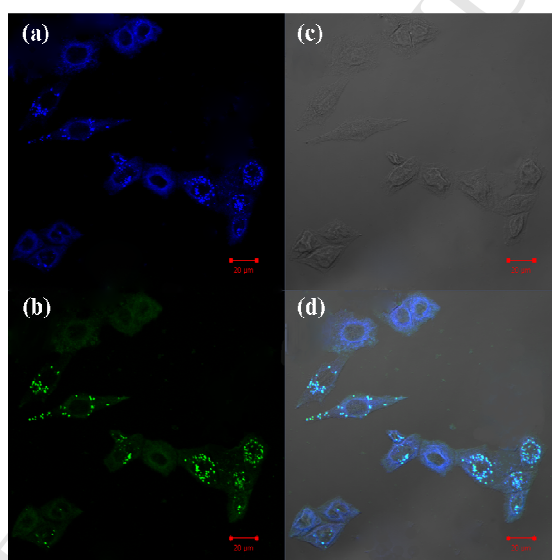


Fig. S34 (a) One-photon fluorescence microscopy image of HepG2 cells stained with **6** with excitation at 405 nm. (b) Two-photon fluorescence microscopy image of HepG2 cells stained with **6** with excitation at 800 nm. (c) Bright-field image. (d) Merged image.